

NPS ARCHIVE
1968
OATES, A.

PROPAGATION OF A SIMPLE TRANSIENT IN AN
ISOVELOCITY LAYER WITH PRESSURE-RELEASE
BOUNDARIES

by

Anthony Brent Oates

UNITED STATES NAVAL POSTGRADUATE SCHOOL



THESIS

PROPAGATION OF A SIMPLE TRANSIENT IN AN
ISOVELOCITY LAYER WITH PRESSURE-RELEASE BOUNDARIES

by

Anthony Brent Oates

June 1968

~~This document is subject to special export con-~~
~~ditions and each transmittal to foreign government~~
~~foreign nationals may be made only with prior~~
~~approval of the U. S. Naval Postgraduate School.~~

LIBRARY
NAVAL POSTGRADUATE SCHOOL
MONTEREY, CALIF. 93940

PROPAGATION OF A SIMPLE TRANSIENT IN AN
ISOVELOCITY LAYER WITH PRESSURE-RELEASE BOUNDARIES

by

Anthony Brent Qates
Lieutenant, United States Navy
B.A., Mathematics, University of Texas, 1961

Submitted in partial fulfillment of the
requirements for the degree of

MASTER OF SCIENCE IN PHYSICS

from the

NAVAL POSTGRADUATE SCHOOL
June 1968

ABSTRACT

The propagation of a simple acoustic transient in an isovelocity water layer was investigated for the purpose of studying the region of validity of a suggested correlation between exact solutions in ducts and solutions for propagation in a layer. The Laplace transform method was used to obtain approximate solutions for the acoustic pressure, particle velocity, and particle displacement resulting from a step-function input in velocity. The radiation impedance characteristics of a Mylar transducer were investigated to study their effect on the received waveforms. Computer programs were written to evaluate and graph the resulting waveforms. The waveforms resulting from a step-function input in velocity were observed and compared with the predicted waveforms. With the use of a family of Mylar transducers, a somewhat doubtful correlation was obtained in the region of validity of the theoretical solutions. Possible causes of the disagreement between the theory and the experiment were investigated. It was found that the theory is believed to be correct, that the experiment was not accurate enough, and that further investigations should be conducted to study the assumed pressure-release characteristics of $\frac{1}{4}$ inch polyethylene.

TABLE OF CONTENTS

Section	Page
1. INTRODUCTION	13
2. THEORETICAL DEVELOPMENT	15
Development of Solutions	15
Transfer Characteristics of Mylar Transducers	22
3. EXPERIMENTAL APPARATUS	37
Tank	37
Transducers	37
Electronic Equipment	40
4. EXPERIMENTAL INVESTIGATION	45
Experimental Procedures	45
Error Analysis	52
5. RESULTS AND CONCLUSIONS	67
6. BIBLIOGRAPHY	68

LIST OF TABLES

Table	Page
2.1 Comparison of Computed Axis Crossings and Amplitudes of Maxima for Acoustic Pressure using Bessel Functions and Trigonometric Approximations to Bessel Functions for the Conditions $r = 91.4$ cm, $a = 4.00$ cm, and $d = 8.00$ cm.	24
2.2 Comparison of Computed Axis Crossings and Amplitudes of Maxima for Acoustic Particle Displacement using Bessel Functions and Trigonometric Approximations to Bessel Functions for the Conditions $r = 91.8$ cm, $a = 6.00$ cm, and $d = 8.00$ cm.	26
3.1 Electronics Equipment.	42

LIST OF ILLUSTRATIONS

Figure	Page
2.1 Acoustic Pressure p vs. Delayed Time t' as Predicted by Computer Programs for the Conditions $r = 91.4$ cm, $a = 4.00$ cm, and $d = 8.00$ cm.	23
2.2 Radial Component of Particle Displacement vs. Delayed Time t' as Predicted by Computer Programs for the Conditions $r = 91.8$ cm, $a = 6.00$ cm, and $d = 8.00$ cm.	25
2.3 Phase Angle and Modulus of Radiation Impedance of a Mylar Transducer used as a Transmitter vs. the Argument of the Hankel Functions, $\frac{a\omega}{c} \sqrt{1 - \left(\frac{\omega_n}{\omega}\right)^2}$	30
2.4 Modulus of Motional Impedance Z_m of the Mylar Transducer used as a Receiver vs. Frequency.	32
2.5 Equivalent Circuit of a Mylar Transducer used as a Receiver.	33
2.6 Phase Angle and Mod $\left[\frac{Z_m + Z_r}{A} \right]^{-1}$ vs. Frequency for Mylar Transducer used as a Receiver.	35
3.1 Laboratory Setup.	39
3.2 Transmitters and Receivers.	39
3.3 Block Diagram of Electronics Equipment.	41
3.4 Load and Bias Network.	44
4.1 Observed Waveforms.	47
4.2 Experimental and Computed t' vs. N/N_a for Acoustic Pressure Waveform Generated by a Step Input in Velocity.	49
4.3 Experimental and Computed t' vs. N/N_a for Particle Displacement Waveform Generated by a Step Input in Velocity for $a = 1.0$ cm.	50
4.4 Experimental and Computed t' vs. N/N_a for Particle Displacement Waveform Generated by a Step Input in Velocity for $a = 6.0$ cm.	51
4.5 Ratio of Experimental to Computed Normalized Acoustic Pressure Amplitudes Generated by a Step Input in Velocity vs. Delayed Time.	53

LIST OF ILLUSTRATIONS (Cont'd)

Figure		Page
4.6	Ratio of Experimental to Computed Normalized Particle Displacement Amplitudes Generated by a Step Input in Velocity vs. Delayed Time for $a = 1.0$ cm.	54
4.7	Ratio of Experimental to Computed Normalized Particle Displacement Amplitudes Generated by a Step Input in Velocity vs. Delayed Time for $a = 6.0$ cm.	55
4.8	Experimental and Computed t'_m vs. N/N_a for Particle Displacement Waveform Generated by a Step Input in Velocity using a One Parameter Fit.	59
4.9	Experimental and Computed t'_m vs. N/N_a for Particle Displacement Waveform Generated by a Step Input in Velocity for Four Positions on the Tank Bottom.	60
4.10	Circuit used to Monitor Current Drawn by Mylar Transducer as a Result of Acoustic Radiation into a Water Medium	62
4.11	Equivalent Circuit of a Mylar Transducer used as a Transmitter.	62
4.12	Bottom Layer Investigation for Three-Layered Bottom and Single-Layered Bottom using 10 cm Source.	63
4.13	Bottom Layer Investigation for Three-Layered Bottom and Single-Layered Bottom using 6 cm Source.	64
4.14	Bottom Layer Investigation for Three-Layered Bottom and Single-Layered Bottom using 4 cm Source.	65

LIST OF SYMBOLS

a	radius of source
c	free field speed of sound in water
$c_p = \frac{c}{\sqrt{1 - (\frac{\omega_n}{\omega})^2}}$	Phase velocity for angular frequency ω in the n th mode
d	depth of the isovelocity layer
n	mode number
r, z, t	cylindrical coordinates, assuming radial symmetry, and time
ω_n	angular cut-off frequency for the n th mode
ρ	density of water
$\Phi = Z(z) \phi(r, t),$	acoustic velocity potential
$\phi(r, t)$	radial portion of velocity potential in layer
$Z(z)$	transverse function in the layer
$p = -\rho \frac{\partial \phi}{\partial t}$	acoustic potential
$u_r = \frac{\partial \phi}{\partial r}$	radial component of particle velocity
ϵ_r	radial component of particle displacement
$I_0(u)$	Modified Bessel function of the first kind
$K_0(u)$	Modified Bessel function of the third kind
$J_n(u)$	Bessel function of the first kind
$\arg = \omega_n \sqrt{t^2 - T^2}$	argument of Bessel functions
$u = \frac{r}{c} \sqrt{\omega_n^2 + \Delta^2}$	argument of Modified Bessel functions
$T = \frac{r-a}{c}$	time of flight of signal from the source at $r = a$ to receiver
$V(t)$	velocity input at $r = a$
δ, ψ	relative phase of the layer solutions with respect to duct solutions
$N = \frac{\omega_n}{2\pi} \sqrt{t^2 - T^2}$	number of cycles of transient generated in time t
N_a	cycle number where the approximations fail to apply

LIST OF SYMBOLS (Cont'd)

$H_n^{(2)}$	Hankel functions of the second kind
$\frac{Z}{\rho} = \frac{p}{u_r}$	specific acoustic impedance
$Z_r = A \underline{Z}$,	radiation impedance where A is the total radiation area of the transducer
Z_m	open-circuit mechanical impedance
s	transducer mechanical stiffness
P_o	atmospheric pressure
l	effective depth of air cushion behind Mylar diaphragm
t	thickness of Mylar
C_o	blocked capacitance of the transducer
C_s	compliance of the transducer
v	signal voltage
\emptyset	turns ratio
R	internal resistance of the power amplifier
V_o	external polarizing voltage
x_o	position of Mylar film when polarizing voltage is applied
P_{ff}	free-field acoustic pressure
$t' = T - t$	delayed time
t'_m	predicted value of axis crossing in layer
t'_{om}	predicted value of axis crossing in duct
t'_{exp}	observed value of axis crossing in layer

ACKNOWLEDGEMENTS

The continuing advice and assistance of Professor Alan B. Coppens of the Naval Postgraduate School is gratefully acknowledged.

Thanks are also due to Mr. William E. Smith for his technical support.

This research was supported in part by the Naval Air Systems Command and the Office of Naval Research.

1. INTRODUCTION

Although most of the current investigations of the propagation of energy in waveguides have been done for electromagnetic cases⁽¹¹⁻¹³⁾, some have considered the propagation of pulsed acoustic energy in waveguides⁽¹⁻⁵⁾. The dispersion of an ultrasonic pulse propagated through a waveguide of circular cross-section filled with water has been used for the approximate determination of the frequency spectrum of the original pulse⁽¹⁾. J. M. Proud et al.⁽²⁾ have shown that the dispersion of a rectangular pulse along an acoustic waveguide of rectangular cross-section can be used to calibrate the waveguide so that it can be used to predict the effects of similar dispersion on the transmission of pulses of other shapes that are not amenable to actual computation. It has been shown, by considering pulse compression in an acoustic waveguide, that a frequency modulated input pulse can be compressed into an output pulse of shorter duration and of higher peak amplitude⁽³⁾. In addition, studies of transient propagation in layered media have been made^(6,7). Many of these studies have used approximation techniques, such as the method of stationary phase, to solve the transient propagation problem. J. R. Wait⁽⁸⁾ has presented a summary of these techniques useful for calculating the resultant propagated waveform. Using the Laplace transform technique, others^(5,9,10) have investigated transient radiation and scattering from cylindrical bodies.

Recently, exact solutions for the propagation of simple transients in waveguides have been published^(4, 11-13). It has been suggested that there is a correlation within a certain region of validity between

exact solutions in ducts and solutions for the propagation of acoustic transients in isovelocity layers^(5,14).

The purpose of this research is to extend investigation of the region of validity of the suggested correlation and of the restrictions under which the solutions describing the transient response of the layer are valid.

2. THEORETICAL DEVELOPMENT

Development of Solutions

The response of an isovelocity layer to simple transient excitations will be developed using the following assumptions:

- (a) cylindrical velocity-source of radius a ,
- (b) constant layer depth d , and
- (c) pressure-release upper and lower boundaries.

The wave equation for acoustic velocity-potential in cylindrical coordinates, under the assumption of radially-symmetric motion, is

$$\left(\frac{\partial^2}{\partial r^2} + \frac{1}{r} \frac{\partial}{\partial r} + \frac{\partial^2}{\partial z^2} - \frac{1}{c^2} \frac{\partial^2}{\partial t^2} \right) \Phi(r, z, t) = 0 \quad 2.1$$

where r is the radial direction and z is the transverse direction.

The convenient separation of variables

$$\Phi(r, z, t) = Z(z) \phi(r, t)$$

casts Eq. 2.1 into

$$\begin{aligned} \left[\frac{\partial^2}{\partial r^2} + \frac{1}{r} \frac{\partial}{\partial r} - \frac{1}{c^2} \frac{\partial^2}{\partial t^2} - \left(\frac{w_n}{c} \right)^2 \right] \phi(r, t) &= 0 \\ \left[\frac{\partial^2}{\partial z^2} + \left(\frac{w_n}{c} \right)^2 \right] Z(z) &= 0 \end{aligned} \quad 2.2$$

where the radial component of the particle velocity becomes

$$u_r = Z(z) \frac{\partial \phi}{\partial r}$$

and the acoustic pressure becomes

$$p = -\rho Z(z) \frac{\partial \phi}{\partial t}.$$

For pressure-release top and bottom, we have $p = 0$ at $z = 0$ and $z = d$; therefore, $Z(z) = D \sin \frac{w_n z}{c}$ where $w_n = \frac{n\pi c}{d}$. Thus, the equation for $Z(z)$, which gives the dependence of the acoustic variables on the layer depth, determines the eigenfrequencies w_n .

These are the cut-off frequencies of the various radially-symmetric normal modes of the layer.

Use of the Laplace transform method to solve Eq. 2.2 with the boundary condition at the source written as

$$u_r(a, t) = Z(z) V(t),$$

which implies excitation of only one mode, casts Eq. 2.2 into the simpler differential equation

$$\left[\frac{d^2}{dr^2} + \frac{1}{r} \frac{d}{dr} - \left(\frac{\omega_n^2 + \Delta^2}{c^2} \right) \right] \bar{\phi}(r, \Delta) = 0 \quad 2.3$$

where $\bar{\phi}(r, s)$ is the Laplace transform of $\phi(r, t)$. $V(t)$ $Z(z)$ is the radial velocity at the source. The relevant boundary conditions become

$$\left. \frac{d\bar{\phi}}{dr} \right|_{r=a} = \bar{V}(\Delta)$$

and

$$\bar{\phi} \rightarrow 0 \text{ as } r \rightarrow \infty.$$

The change of variable $u = \frac{r}{c} \sqrt{\omega_n^2 + s^2}$ casts Eq. 2.3 into the form

$$\frac{d^2 \bar{\phi}}{du^2} + \frac{1}{u} \frac{d\bar{\phi}}{du} - \bar{\phi} = 0 \quad 2.4$$

which has solution⁽¹⁵⁾

$$\bar{\phi} = A I_0(u) + B K_0(u)$$

where I_0 and K_0 are the modified Bessel functions. Since $I_0(u) \rightarrow \infty$ and $K_0(u) \rightarrow 0$ as $u \rightarrow \infty$, the solution to Eq. 2.4 which obeys the required boundary conditions is

$$\bar{\phi} = C(\Delta) K_0(u)$$

where

$$C(\Delta) = \bar{V}(\Delta) \frac{c}{\sqrt{\rho^2 + \omega_n^2}} \frac{1}{K_1\left(\frac{a}{c} \sqrt{\rho^2 + \omega_n^2}\right)}.$$

Under the Laplace transform, the acoustic pressure, radial component of particle velocity, and radial component of particle displacement become

$$\frac{\bar{p}}{\rho c Z(z)} = \bar{V}(\lambda) \frac{\lambda}{\sqrt{\lambda^2 + \omega n^2}} \frac{K_0\left(\frac{\lambda}{c} \sqrt{\lambda^2 + \omega n^2}\right)}{K_1\left(\frac{a}{c} \sqrt{\lambda^2 + \omega n^2}\right)}$$

$$\frac{\bar{u}_r}{Z(z)} = \bar{V}(\lambda) \frac{K_1\left(\frac{\lambda}{c} \sqrt{\lambda^2 + \omega n^2}\right)}{K_1\left(\frac{a}{c} \sqrt{\lambda^2 + \omega n^2}\right)}$$

$$\frac{\bar{\xi}_r}{Z(z)} = \frac{\bar{V}(\lambda)}{\lambda} \frac{K_1\left(\frac{\lambda}{c} \sqrt{\lambda^2 + \omega n^2}\right)}{K_1\left(\frac{a}{c} \sqrt{\lambda^2 + \omega n^2}\right)}$$

Formal inversion results in expressions like

$$u_r = \frac{Z(z)}{2\pi i} \int_{-i\infty}^{+i\infty} \bar{V}(\lambda) \frac{K_1\left(\frac{\lambda}{c} \sqrt{\lambda^2 + \omega n^2}\right)}{K_1\left(\frac{a}{c} \sqrt{\lambda^2 + \omega n^2}\right)} e^{\lambda t} d\lambda \quad 2.5$$

where the contour is indented into the right half-plane around the singularities on the imaginary axis. Exact solutions to Eq. 2.5 do not appear to be known, but certain approximations may be used to obtain approximate solutions for the leading portions of the propagating transient.

For large values of argument, use of standard approximations⁽¹⁵⁾ for the modified Bessel functions results in the following asymptotic form

$$\frac{K_n\left(\frac{\lambda}{c} \sigma\right)}{K_m\left(\frac{a}{c} \sigma\right)} \doteq \sqrt{\frac{a}{\lambda}} e^{-\pi \sigma} \left\{ 1 + A_{nm}\left(\frac{c}{a\sigma}\right) + B_{nm}\left(\frac{c}{a\sigma}\right)^2 + C_{nm}\left(\frac{c}{a\sigma}\right)^3 + \dots \right\} \quad 2.6$$

where $\sigma = \sqrt{w_n^2 + \Delta^2}$ and $T \equiv \frac{r-a}{c}$,

and

$$A_{01} = -\left(\frac{3}{8} + \frac{1}{8} \frac{a}{r}\right)$$

$$B_{01} = \frac{33}{128} + \frac{6}{128} \frac{a}{r} + \frac{9}{128} \left(\frac{a}{r}\right)^2$$

$$A_{11} = -\frac{3}{8} \left(1 - \frac{a}{r}\right)$$

$$B_{11} = \frac{33}{128} - \frac{18}{128} \frac{a}{r} - \frac{15}{128} \left(\frac{a}{r}\right)^2,$$

The symbol T represents the time of flight over the shortest path between the surface of the source and the field point. The restriction on s necessary to satisfy the approximation which led to Eq. 2.6 is

$$\left| \frac{a}{c} \sigma \right| \geq 1.$$

Imaginary s greater than w_n in magnitude requires

$$\left| \frac{\Delta}{c} \right| \geq w_a$$

where

$$w_a = w_n \sqrt{1 + \left(\frac{c}{a w_n}\right)^2}$$

is clearly a function of the source-radius and the cut-off frequency for the mode of interest. For a waveguide with pressure-release boundaries which is excited in the lowest mode, the quantity $\frac{w_n a}{c}$ has the value $\frac{\pi a}{d}$ which demonstrates the importance of the ratio of source-radius to layer-depth. As a result of the approximation which led to Eq. 2.6, Eq. 2.5 can be broken into two parts:

$$\begin{aligned} \frac{U_r}{z(z)} 2\pi L = & \int_{\left|\frac{\Delta}{c}\right| \geq w_a} \sqrt{\frac{a}{r}} \left[1 + A_{11} \left(\frac{\Delta}{a\sigma}\right) + B_{11} \left(\frac{\Delta}{a\sigma}\right)^2 + \dots \right] e^{st - T\sigma} \frac{w_n}{V} d\Delta \\ & + \int_{-i w_a}^{+i w_a} \frac{1}{V} \left[\frac{K_1 \left(\frac{\pi}{2} \sigma\right)}{K_1 \left(\frac{a}{c} \sigma\right)} \right] e^{\Delta t} d\Delta. \end{aligned}$$

Each portion contributes significantly to u_r only when the exponent of each is stationary. For large s (which corresponds to the leading portion of the signal), only the first integral is important and yields its major contribution when the exponent has a vanishing derivative

$$\frac{d}{ds}(\Delta t - T\sigma) = 0 = t - \frac{\Delta_0 T}{\sqrt{\Delta_0^2 + \omega n^2}}.$$

Thus, the requirement that $|\Delta_0/i| \geq \omega a$ sets an upper limit

$$t_a = T \sqrt{1 + \left(\frac{a\omega n}{c}\right)^2}$$

on the time within which the first integral yields the major contribution.

For a step input, for which $\bar{V}(s) = \frac{1}{s}$, the radial component of the particle displacement becomes

$$\frac{\xi_r}{z(z)} = \frac{1}{\Delta^2} \frac{K_1\left(\frac{r}{c} \sqrt{\Delta^2 + \omega n^2}\right)}{K_1\left(\frac{a}{c} \sqrt{\Delta^2 + \omega n^2}\right)}.$$

Application of the asymptotic approximations of Eq. 2.6 leads to

$$\frac{\xi_r}{z(z)} \doteq \frac{1}{\Delta^2} \sqrt{\frac{a}{r}} e^{-T\sigma} \left\{ 1 + A_{11} \left(\frac{c}{a\sigma}\right) + B_{11} \left(\frac{c}{a\sigma}\right)^2 + \dots \right\}.$$

Inversion⁽⁵⁾ leads to

$$\begin{aligned} \frac{\xi_r}{z(z)} \doteq & \sqrt{\frac{a}{r}} \left\{ \frac{2}{a\omega n} \sum_{m=1}^{\infty} (2m-1) \left(\frac{t-T}{t+T}\right)^{\frac{2m-1}{2}} J_{2m-1}(\arg) \right. \\ & + A_{11} \frac{2}{\omega n} \left(\frac{c}{a\omega n}\right) \sum_m (2m) \left(\frac{t-T}{t+T}\right)^m J_{2m}(\arg) \\ & + B_{11} \frac{2}{\omega n} \left(\frac{c}{a\omega n}\right)^2 \left[\sum_m (2m-1) \left(\frac{t-T}{t+T}\right)^{\frac{2m-1}{2}} J_{2m-1}(\arg) \right. \\ & \left. \left. - \sum_m (-1)^{m-1} \left(\frac{t-T}{t+T}\right)^{\frac{2m-1}{2}} J_{2m-1}(\arg) \right] \right\} \end{aligned} \quad 2.7$$

where $\arg = \omega_n \sqrt{t^2 - T^2}$.

For a step input, the solution for the acoustic pressure becomes

$$\begin{aligned} \frac{p}{\rho c z(z)} \doteq & \sqrt{\frac{a}{r}} \left\{ J_0(\arg) + A_{01} \frac{2c}{a\omega n} \sum_{m=1}^{\infty} (-1)^{m-1} \left(\frac{t-T}{t+T}\right)^{\frac{2m-1}{2}} \right. \\ & \left. J_{2m-1}(\arg) + B_{01} \left(\frac{2c}{a\omega n}\right)^2 \sum_m (-1)^{m-1} m \left(\frac{t-T}{t+T}\right)^m J_{2m}(\arg) \right\}. \end{aligned} \quad 2.8$$

The quantity $t' = t - T$ appearing in Eqs. 2.7 and 2.8 represents the time which has elapsed since the propagating transient signal traveling with velocity c first arrived at the position r . This quantity will be denoted as the "delayed time".

For the leading portion of the propagating transient, one can apply a standard trigonometric asymptotic approximation⁽¹⁵⁾

$$J_Y(y) = \sqrt{\frac{2}{\pi y}} \cos\left(y - \frac{\pi}{4} - \frac{2\pi}{2}\right) \quad 2.9$$

to the functions in Eqs. 2.7 and 2.8. Application of this approximation to the sums of Eqs. 2.7 and 2.8 leads to expressions of the types

$$\sqrt{\frac{2}{\pi y}} \sum_{n=0}^{\infty} e^{2n+1} \cos\left(y - \frac{\pi}{4} - n\pi - \frac{2\pi}{2}\right) \rightarrow \sqrt{\frac{2}{\pi y}} \frac{e^1}{1+e^2} \cos\left(y - \frac{\pi}{4} - \frac{2\pi}{2}\right)$$

$$\sqrt{\frac{2}{\pi y}} \sum_n e^{4n+1} \cos\left(y - \frac{\pi}{4} - \frac{2\pi}{2}\right) \rightarrow \sqrt{\frac{2}{\pi y}} \frac{e^1}{1+e^4} \cos\left(y - \frac{\pi}{4} - \frac{2\pi}{2}\right). \quad 2.10$$

Application of Eqs. 2.9 and 2.10 to the solution for particle displacement casts it in the form

$$\frac{\xi_r}{z(z)} \rightarrow \sqrt{\frac{a}{r}} \frac{1}{\pi} \frac{1}{\sqrt{N}} \frac{1}{t} \left[\frac{\sqrt{t^2 - \pi^2}}{w_n t} \right] \left\{ \left[1 - B_{11} \left(\frac{N}{N_a} \right)^2 \right] \cos\left(2\pi N - \frac{\pi}{4} - \frac{\pi}{2}\right) + A_{11} \left(\frac{N}{N_a} \right) \sin\left(2\pi N - \frac{\pi}{4} - \frac{\pi}{2}\right) \right\}. \quad 2.11$$

where $2\pi N = y$ and $N_a = \frac{1}{2} w_n T \frac{a w_n}{c}$.

The quantity N is the number of cycles of the transient generated in time t , and N_a corresponds to the cycle where the approximations (and thus the theory) fail to apply.

By combining the sine and cosine terms of Eq. 2.11, we find the expression for the radial component of particle displacement to be

$$\frac{\xi_r}{z(z)} \rightarrow \sqrt{\frac{a}{r}} \frac{1}{\pi} \frac{1}{\sqrt{N}} \frac{T}{t} \left[\frac{\sqrt{t^2 - T^2}}{wnt} \right] C(t) \sin(2\pi N - \frac{\pi}{4} + \psi) \quad 2.12$$

where $C(t) = \sqrt{\left[1 - B_{11}\left(\frac{N}{N_a}\right)^2\right]^2 + \left[A_{11}\frac{N}{N_a}\right]^2}$ and

$$\tan \psi = - \frac{A_{11} \frac{N}{N_a}}{1 - B_{11}\left(\frac{N}{N_a}\right)^2}.$$

Application of Eqs. 2.9 and 2.10 to the solution for acoustic pressure casts it in the form

$$\frac{p}{p_0 z(z)} = \sqrt{\frac{a}{r}} \frac{1}{\pi} \frac{1}{\sqrt{N}} A(t) \cos\left(2\pi N - \frac{\pi}{4} + \gamma\right) \quad 2.13$$

where $A(t) = \sqrt{\left[1 - B_{01}\left(\frac{N}{N_a}\right)^2\right]^2 + \left[A_{01}\left(\frac{N}{N_a}\right)\right]^2}$ and

$$\tan \gamma = - \frac{A_{01}\left(\frac{N}{N_a}\right)}{1 - B_{01}\left(\frac{N}{N_a}\right)^2}.$$

Previous work^(5,14) has shown that for the same input as above the exact solution for propagation of a transient in a duct becomes the leading term in the solution developed for the isovelocity layer. It should be noted that these duct terms can be retrieved from the trigonometric approximations by letting the amplitude factors go to unity and the phase angles go to zero.

The solutions, using Bessel functions or asymptotic approximations to the Bessel functions, for the transient response of an isovelocity layer have been developed with the restriction

$$T \leq t \leq t_a \quad \text{or} \quad N/N_a \leq 1.$$

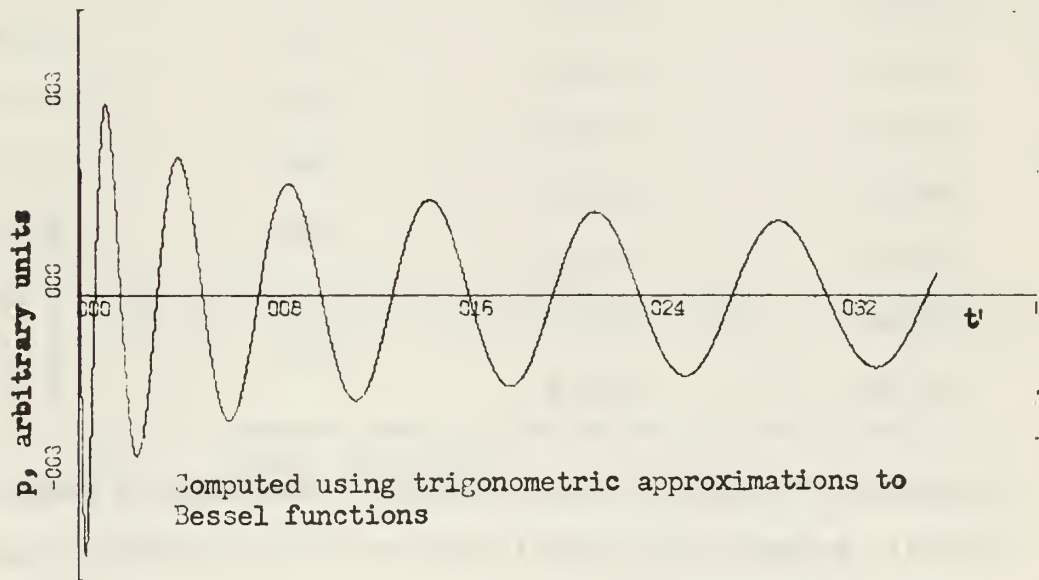
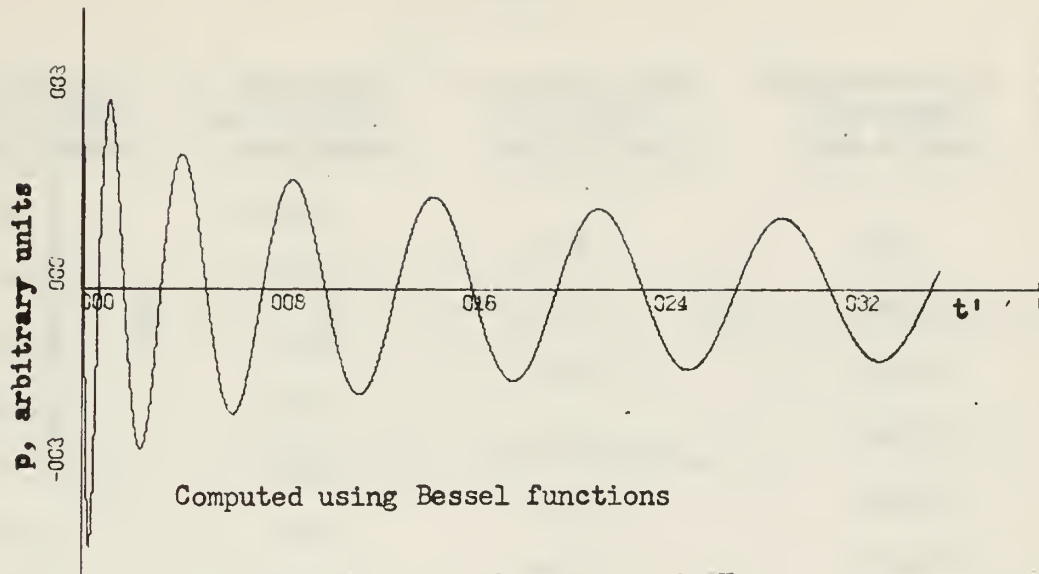
Computer programs have been written to evaluate the predicted waveforms for acoustic pressure and particle displacement, using either the Bessel function or trigonometric approximations (see Appendices A and B, respectively). These programs give printed and graphical outputs for the duct and layer terms. In addition,

these programs predict the axis-crossings and amplitude-modulation in the layer. Figures 2.1 and 2.2 illustrate the acoustic pressure and particle displacement, respectively, predicted by the two approximations. Tables 2.1 and 2.2 give the calculated values of the predicted axis-crossings and amplitude-modulation for acoustic pressure and particle displacement. It should be noted that the first portion of the first half-cycle of the waveform predicted by the trig computer program is not accurate. To avoid a mathematical ambiguity at the leading portion of the waveform, its value has been set equal to zero. For comparison purposes, the predicted amplitude peaks were normalized to the value of the highest peak in the waveform. As can be seen from a study of Tables 2.1 and 2.2, the difference between the two predictions is on the order of one per cent which is smaller than the experimental accuracy encountered. Therefore, the predictions from the computer program using trigonometric approximations will be used for all comparisons with experimental data.

The approximate solutions for the propagation of a transient in an isovelocity layer have been developed, and computer programs to evaluate these solutions and predict the axis-crossings and amplitude-modulation in the layer have been written.

Transfer Characteristics of Mylar Transducers

To have some measure of confidence in the received waveform, it was decided to investigate the transfer characteristics, under steady-state conditions, for Mylar transducers. This investigation will cover the radiation impedance at the surface of the transmitter, $r = a$, and the radiation impedance of a receiver.



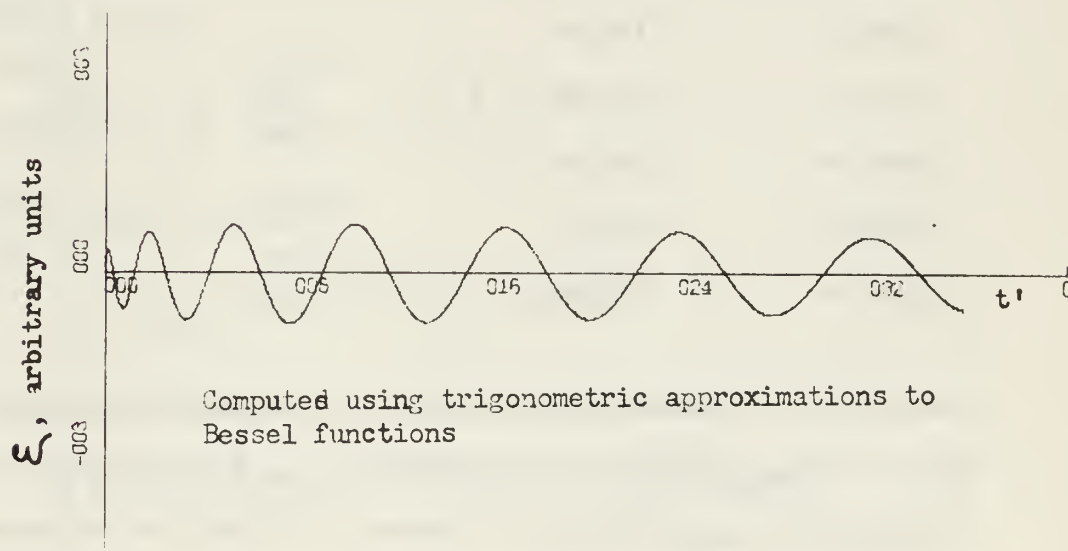
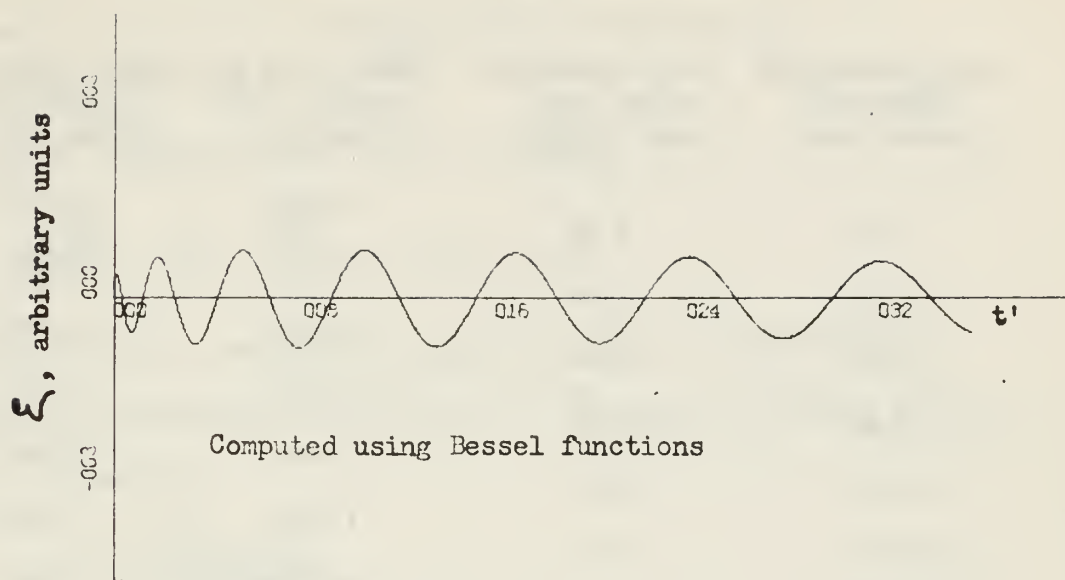
Acoustic Pressure p vs. Delayed Time t' as Predicted by Computer Programs for the Conditions $r=91.4$ cm, $a=4.00$ cm and $d=8.00$ cm.

Figure 2.1

Table 2.1

AXIS CROSSINGS USING BES TIME IN USEC	AXIS CROSSINGS USING TRIG TIME IN USEC	AMPLITUDES OF MAXIMA, BES NORMALIZED	AMPLITUDES OF MAXIMA, TRIG NORMALIZED
		1.000	1.000
1.45	1.39		
		0.632	0.647
7.53	7.46		
		0.470	0.478
18.32	18.26		
		0.390	0.396
33.58	33.51		
		0.339	0.344
52.99	52.91		
		0.303	0.308
76.17	76.08		
		0.275	0.280
102.72	102.64		
		0.253	0.258
132.33	132.21		
		0.235	0.239
164.57	164.42		
		0.219	0.224
199.13	198.96		
		0.205	0.210
235.72	235.51		
		0.193	0.198
274.07	273.82		
		0.182	0.186
313.96	313.65		
		0.171	0.177
355.18	354.81		

Comparison of computed axis-crossings and amplitudes of maxima for acoustic pressure using Bessel functions and trigonometric approximations to Bessel functions for the conditions $r = 91.4$ cm, $a = 4.00$ cm, and $d = 8.00$ cm.



Radial Component of the Particle Displacement ξ vs. Delayed Time t'
 Predicted by Computer Programs for the Conditions $r=91.8$ cm, $a=6.00$ cm,
 and $d=8.00$ cm.

Figure 2.2

Table 2.2

AXIS CROSSINGS USING BES TIME IN USEC	AXIS CROSSINGS USING TRIG TIME IN USEC	AMPLITUDES OF MAXIMA, BES NORMALIZED	AMPLITUDES OF MAXIMA, TRIG NORMALIZED
3.75	3.92	0.474	0.475
12.48	12.60	0.701	0.698
25.94	25.99	0.844	0.841
43.82	43.79	0.933	0.931
65.75	65.64	0.982	0.981
91.33	91.13	1.000	1.000
120.16	119.89	0.995	0.996
151.85	151.51	0.974	0.975
186.05	185.65	0.941	0.943
222.44	221.99	0.901	0.903
260.73	260.24	0.857	0.860
300.68	300.15	0.811	0.814
342.07	341.50	0.764	0.768

Comparison of computed axis-crossings and amplitudes of maxima for the acoustic particle displacement using Bessel functions and trigonometric approximations to Bessel functions for the conditions $r = 91.8$ cm, $a = 6.00$ cm, and $d = 8.00$ cm.

In a steady-state condition, the acoustic potential for a cylindrical source in a waveguide can be expressed as

$$\phi_r = Z(z) R(r) e^{i\omega t}. \quad 2.14$$

The time independent wave equation becomes

$$\frac{d^2 \phi_r}{dr^2} + \frac{1}{r} \frac{d\phi_r}{dr} + k^2 \phi_r = 0.$$

The separation of variables suggested in Eq. 2.14 leads to the value of the separation constant, $k_r = \frac{\omega}{c_p}$, where the phase velocity c_p is defined as

$$c_p = \frac{c}{\sqrt{1 - \left(\frac{\omega n}{\omega}\right)^2}}. \quad 2.15$$

Thus, the wave equation for the radial component of the acoustic potential becomes

$$\frac{d^2 R}{dr^2} + \frac{1}{r} \frac{dR}{dr} + k_r^2 R = 0$$

with the general solution

$$R(r) = \underline{A} J_0(k_r r) \pm \underline{B} Y_0(k_r r). \quad 2.16$$

For an outward traveling wave, Eq. 2.16 becomes

$$\underline{R}(r) = A [J_0(k_r r) - i Y_0(k_r r)] = A H_0^{(2)}(k_r r). \quad 2.17$$

The acoustic potential, acoustic pressure, and the radial component of the particle velocity become

$$\begin{aligned} \frac{\phi_r}{Z(z)} &= H_0^{(2)}\left(\frac{\omega r}{c_p}\right) e^{i\omega t} \\ \frac{p_r}{Z(z)} &= -i\omega p H_0^{(2)}\left(\frac{\omega r}{c_p}\right) e^{i\omega t} \\ \frac{u_r}{Z(z)} &= -H_1^{(2)}\left(\frac{\omega r}{c_p}\right) \left(\frac{\omega}{c_p}\right) e^{i\omega t}. \end{aligned}$$

Using Eq. 2.15, the specific acoustic impedance \underline{Z} becomes

$$\underline{Z} = \frac{p_r}{u_r} = i \rho c_p \frac{H_0^{(2)}(\arg)}{H_1^{(2)}(\arg)} \quad 2.18$$

$$\text{where } \arg = \frac{wr}{c} \sqrt{1 - \left(\frac{w_n}{w}\right)^2}.$$

Then, the radiation impedance Z_r is given by

$$Z_r = A \underline{Z} = i \rho c_p A \frac{H_0^{(2)}(\arg)}{H_1^{(2)}(\arg)}.$$

where A is the total radiation area of the transducer. Thus, the radiation impedance at the surface of the transducer, $r = a$, is given by

$$Z_r = \frac{i \rho c A}{\sqrt{1 - \left(\frac{w_n}{w}\right)^2}} \frac{H_0^{(2)}\left(\frac{wa}{c} \sqrt{1 - \left(\frac{w_n}{w}\right)^2}\right)}{H_1^{(2)}\left(\frac{wa}{c} \sqrt{1 - \left(\frac{w_n}{w}\right)^2}\right)}. \quad 2.19$$

The behavior of Eq. 2.19 as a function of frequency will be investigated. An estimate of the maximum frequency encountered in a shallow-water layer can be derived by recalling that the highest frequencies in the transient occur in the first half-cycle. The following relation concerning the time for the maximum frequency can be derived:

$$w_n \sqrt{t_{\max}^2 - \tau^2} = 2\pi N = \pi \quad \text{or}$$

$$t_{\max}^2 = \tau^2 + \frac{1}{(2fn)^2} \quad \text{where } 2fn = \frac{c}{d}.$$

The relation for the instantaneous frequency

$$w = \frac{w_n t}{\sqrt{t^2 - \tau^2}}$$

can then be manipulated into the desired result

$$w_{\max} = \sqrt{1 + \left(\frac{r-a}{d}\right)^2}.$$

For $r-a = 100$ cm and $d = 8$ cm,

$$w_{\max} = 650 \text{ khz.}$$

The cut-off frequency for the first mode and the above approximations is

$$w_n = 59 \text{ khz.}$$

Thus, the range of frequencies expected to be encountered are

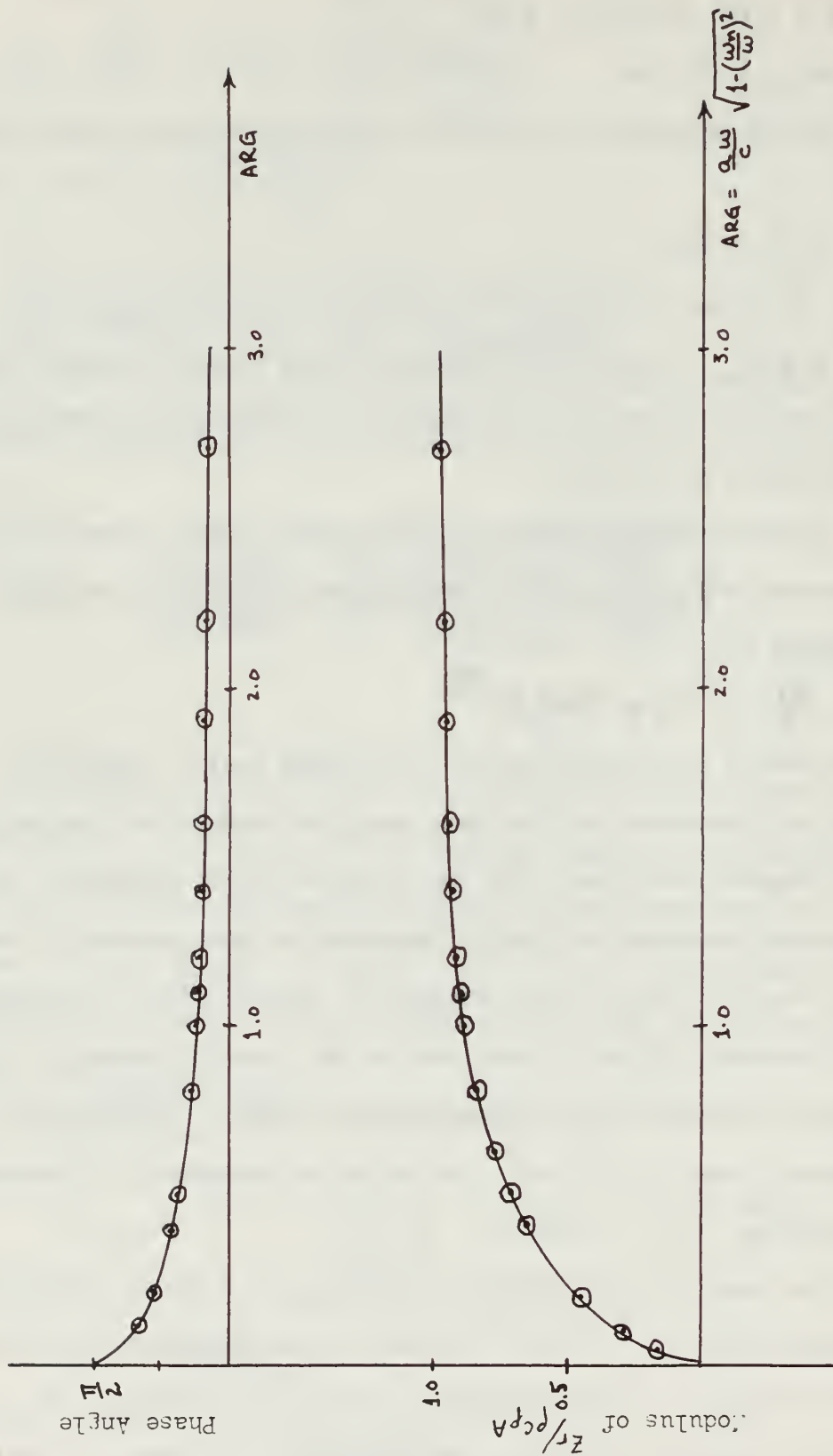
$w_n < w \leq w_{\max}$. The expected frequency must always be greater than the lower limit, for the assumption of a steady state condition no longer holds at $w = w_n$.

Since the Hankel functions are complex numbers, they can be expressed as a modulus and a phase angle. Thus, Eq. 2.19 can be rewritten as

$$\frac{Z_r}{A} = \rho c_p \text{Mod } e^{i\theta}$$

where Mod is the modulus and θ is the phase angle. Figure 2.3 shows the dependence of the phase angle and modulus on the argument of the Hankel functions. For small values of the arguments, the radiation impedance is strongly dependent on the frequency. However, when the value of the argument is about π which corresponds to a frequency within 0.5 per cent of the cut-off frequency, the radiation impedance can be approximated by $A\rho c$. Thus, for the frequency range of interest, the radiation impedance is frequency independent.

The open-circuit mechanical impedance of a Mylar transducer⁽¹⁶⁾ is given by $Z_m = r + i(\omega m - s/\omega)$ where r is the transducer mechanical resistance and s is the transducer mechanical stiffness. For the frequency range of interest, the mechanical resistance is considered to be negligible in comparison with the reactive part of Z_m . Under



Phase Angle and Modulus of Radiation Impedance of a Mylar Transducer used as a Transmitter vs. the Argument of the Hankel Functions, $\frac{w}{c} \sqrt{1 - \left(\frac{w}{w_0}\right)^2}$.

Figure 2.3

the assumption that the mechanical stiffness is given by⁽¹⁶⁾

$s = P_o A / \lambda$ where P_o is the atmospheric pressure and λ is the effective depth of the air cushion behind the Mylar diaphragm, the equation for Z_m can be rewritten as

$$Z_m = i A [\omega \rho_{\text{MYLAR}} t - P_o / \lambda \omega]$$

where t is the thickness of the Mylar. With the nominal values

$$\rho_{\text{mylar}} = 1.395 \text{ gm/cm}^3,$$

$$t = 2.54 \times 10^{-3} \text{ cm},$$

$$P_o = 1.013 \times 10^6 \text{ dyne/cm}^2, \text{ and}$$

$$\lambda = 2.00 \times 10^{-3} \text{ cm},$$

the values of Z_m for the frequency range of interest can be calculated. Figure 2.4 shows the dependence of the magnitude of $\frac{Z_m}{A}$ vs. frequency.

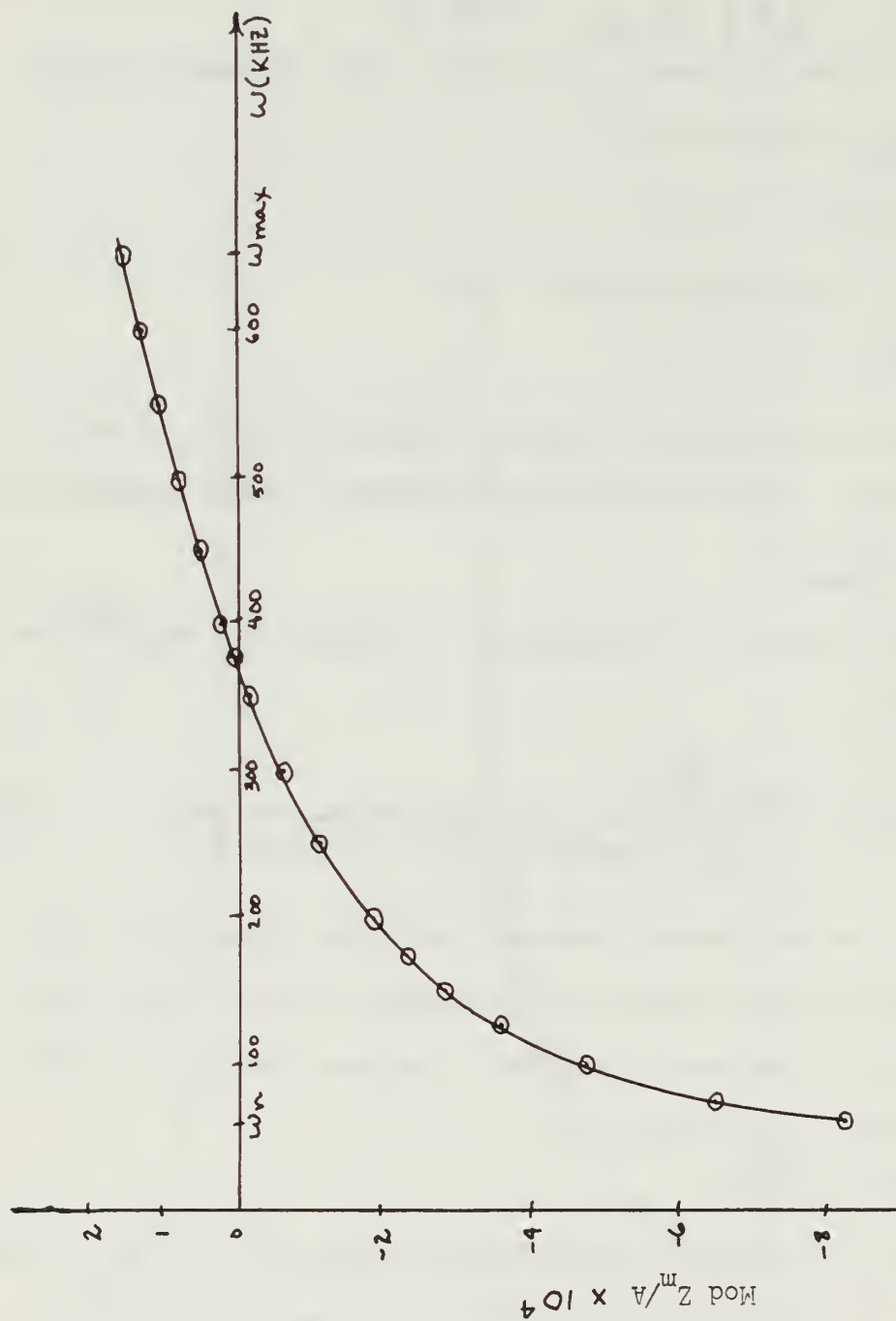
The velocity of the diaphragm of a Mylar transducer⁽¹⁶⁾ is given by

$$u = \frac{i \omega v \phi C_o}{-\omega^2 R C_o^2 (Z_m + Z_r) - \phi^2 + i \omega C_o (Z_m + Z_r)} \quad 2.20$$

where C_o is the blocked diaphragm electrical capacitance, v is the signal voltage across the transducer, ϕ is the turns ratio, and R is the internal resistance of the power amplifier. The turns ratio ϕ is defined as

$$\phi = \frac{C_o V_o}{x_o}$$

where V_o is the external polarizing voltage and x_o is the position of the Mylar film when the polarizing voltage is applied. A comparison of the magnitudes of the terms in the denominator of



Modulus of Motional Impedance Z_m of the Mylar Transducer used as a Receiver vs. Frequency.

Figure 2.4

Using Eq. 2.19 to determine the radiation impedance of the transducer and rewriting the quantity $(Z_m + Z_r)$ as a modulus and a phase angle, one can determine that the open-circuit voltage for a receiver can be written as

$$V = \frac{P_{eff}}{\phi^2 e^{-j\theta}} = \frac{j\omega C_0 \text{Mod} \left(\frac{A}{Z_m + Z_r} \right)}{2.22}$$

Figure 2.6 shows the dependence of the phase angle and $1/\text{Mod} \left(\frac{A}{Z_m + Z_r} \right)$ vs. frequency. As can be seen, the effect of the modulus must be taken into account when comparing the magnitude of the observed signal with that predicted by the theory. The phase angle is constant until the last portion of the signal, but it must be considered at that time.

As discussed earlier, the radiation impedance can be approximated by $A\rho c$, and the free-field pressure can be replaced by $Z_r u_r$. Thus, Eq. 2.22 can be cast into the form

$$V \propto \frac{A\rho c u_r \phi^2 e^{-j\theta}}{j\omega C_0 \text{Mod} (Z_m + Z_r)}$$

Since $u_r = i\omega Z_r$, the open-circuit voltage can be rewritten to indicate its proportionality to the particle displacement

$$V \propto \frac{Z_r}{\text{Mod} (Z_m + Z_r)} \quad 2.23$$

By considering the radiation impedance of a Mylar transducer, assuming steady state conditions, it has been shown that the diaphragm velocity at the transmitter is a mirror of the input voltage and that the open-circuit voltage of a Mylar transducer used as a receiver

Eq. 2.20 using the nominal values: $V_o = 225$ volts, $v = 20$ volts, $C_o = .020$ uF, and $R = 10^{-3}$ ohms, shows that the diaphragm velocity at $r = a$ can be approximated by

$$u \propto \frac{v \phi}{(z_m + z_r)}.$$

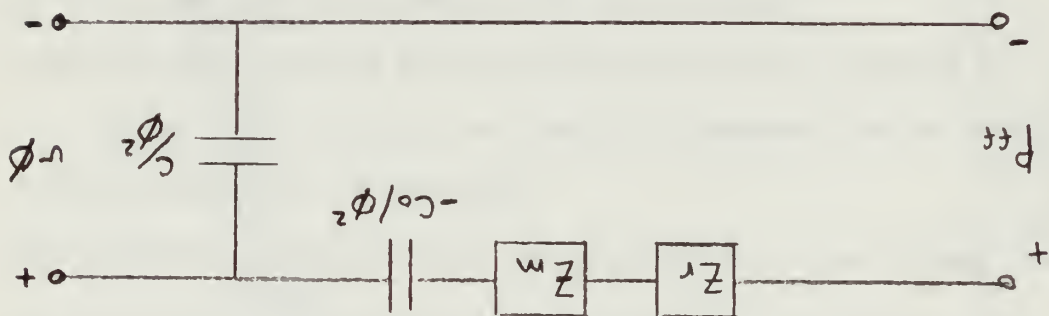
2.21

Thus, for constant $(z_m + z_r)$, the diaphragm velocity is a mirror of the input voltage.

As a receiver, the Mylar film is set into motion by an

impinging sound pressure wave. The equivalent circuit of the

transducer is shown in Fig. 2.5.



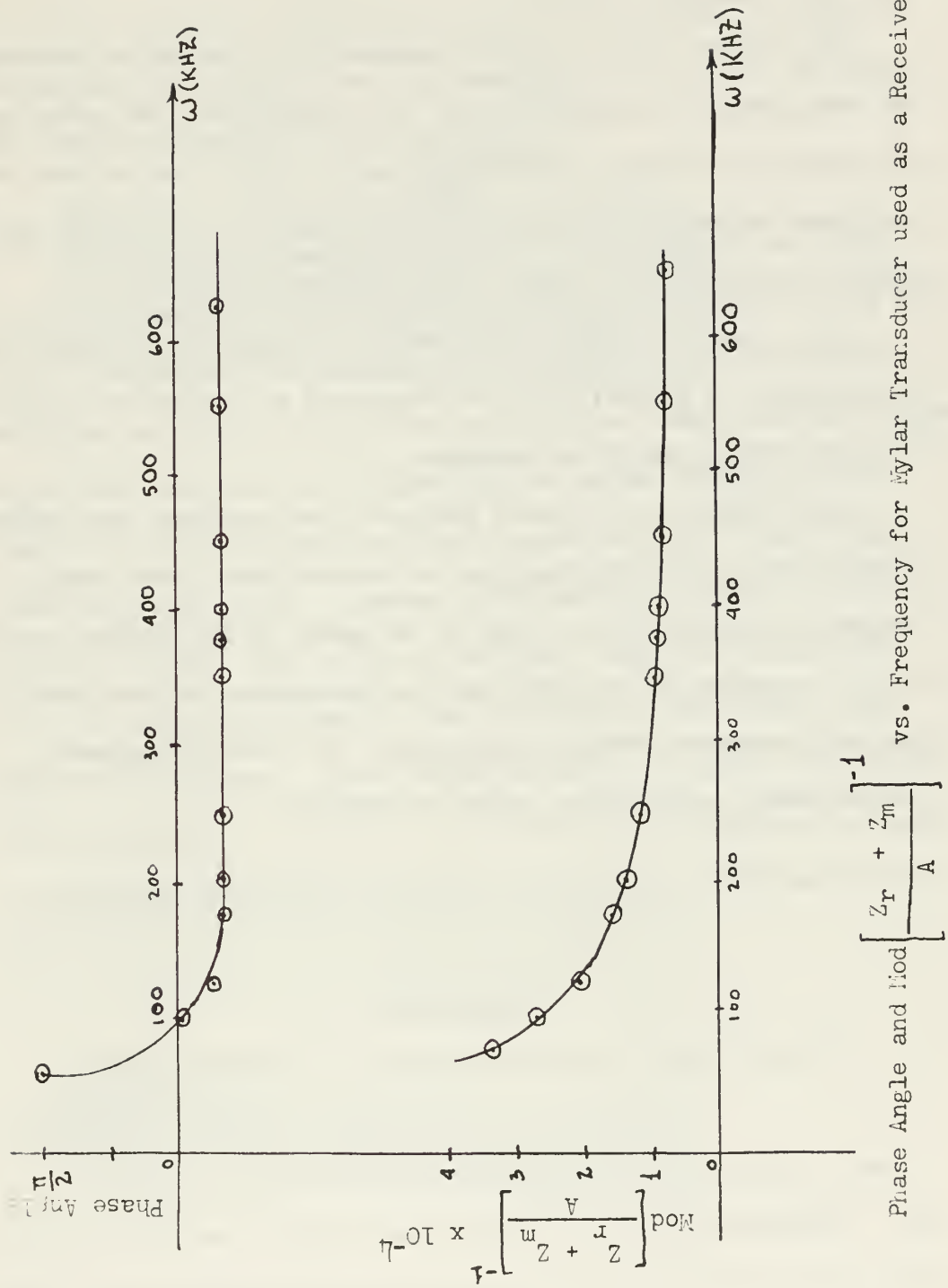
Equivalent Circuit of a Mylar Transducer used as a Receiver

Figure 2.5

The open-circuit voltage developed at the right-hand port is a result of the voltage divider action across the shunt capacitor

$\frac{C}{C_o}$, so that

$$\frac{V}{P_{eff}} = \frac{A \phi^2}{i \omega C_o (z_m + z_r)}.$$



vs. Frequency for Mylar Transducer used as a Receiver.

Figure 2.6

is proportional to the particle displacement. These conclusions only hold for the leading portions of the received transient where Z_r can be replaced by $A\rho c$.

The effect of the transfer characteristics of Mylar transducers has been found to be dependent on the frequency and the radius of the transducer. Given a transient signal which is the mirror of the input voltage, the following is a summary of the effects that would be observed as a result of the radiation impedance:

(a) since the radii of the family of transmitters were large, the response is essentially flat throughout the region of interest; thus, no effects should be observed.

(b) because of the small radius of the receiver, the effect becomes more pronounced than for the transmitters. One should observe a reduction in the size of the peaks of the leading portion of the transient and should observe an enhancement of the peaks as the local apparent frequency approaches the cut-off frequency. A similar phase angle effect should be observed.

3. EXPERIMENTAL APPARATUS

The experimental apparatus in this research project consisted of a tank, a family of cylindrical Mylar transducers, a barium titanate array receiver, and the associated electronics equipment. The laboratory setup is shown in Fig. 3.1.

Tank

The water layer was contained in a tank constructed of 5/8 inch marine plywood. The dimensions of the tank were 6 ft x 6 ft x 1 ft. The plywood was covered with Varathene to provide waterproofing and lined with 1/4 inch polyethylene foam which was assumed to provide the desired pressure-release bottom boundary of the layer. The polyethylene, not being waterproof, was coated with liquid Neoprene paint to prevent deterioration of the pressure-release surface. The bottom of the water layer was maintained level by means of adjustable feet installed in the legs of the supporting platform. Since the walls of the tank were also lined with polyethylene, the tank could be excited as a pressure-release cavity, which provided one method of determining the depth of the layer.

Transducers

Previous work^(5,16) had indicated that Mylar dielectric transducers were well-suited for use in layers.

A family of eight Mylar transducers and one barium titanate linear array were constructed for use in this investigation. The radii of the Mylar transducers were 10 cm, 6 cm, 4 cm, 2 cm, 1 cm, 0.5 cm, and two at 0.25 cm. Each had an active radiating face

8 cm in height which was the maximum depth of the layer. These various transducer dimensions were chosen to provide a large range of values for the ratio N/N_a . The barium titanate array was 8 cm high and 1/8 inch in diameter.

The Mylar transducers were constructed using techniques described in ⁽¹⁶⁾, modified as follows:

(a) The backplates of the larger transducers were constructed from $\frac{1}{2}$ inch thick aluminum cylinders. The backplates for the smallest transducers were fabricated from $\frac{1}{4}$ inch diameter copper tubing.

(b) The cylinders were capped at the top and bottom by lucite plates.

(c) The Mylar film was cut to the desired dimensions and attached to the aluminum cylinders with thin strips of double-stick tape, one piece around the top, one around the bottom, and one piece vertically from bottom to top.

(d) The inner electrical connection was made from the center pin of a BNC connector mounted in the center of the top lucite plate to the inside of the backplate. The outer conducting path from the metallized side of the Mylar film to the BNC was completed by covering the top lucite plug with aluminum foil which was lapped over the Mylar film. To ensure good electrical continuity, silver paint was applied to the aluminum-Mylar interface. To decrease the possibility of electrical pickup, the bottom lucite plate was also covered with aluminum foil.

(e) When the silver paint had dried, the entire transducer was covered with liquid neoprene to provide the necessary waterproofing.



Tank with transmitter and receiver. Electronics equipment in the background.

Laboratory Setup

Figure 3.1



Transmitters and Receivers.

Figure 3.2

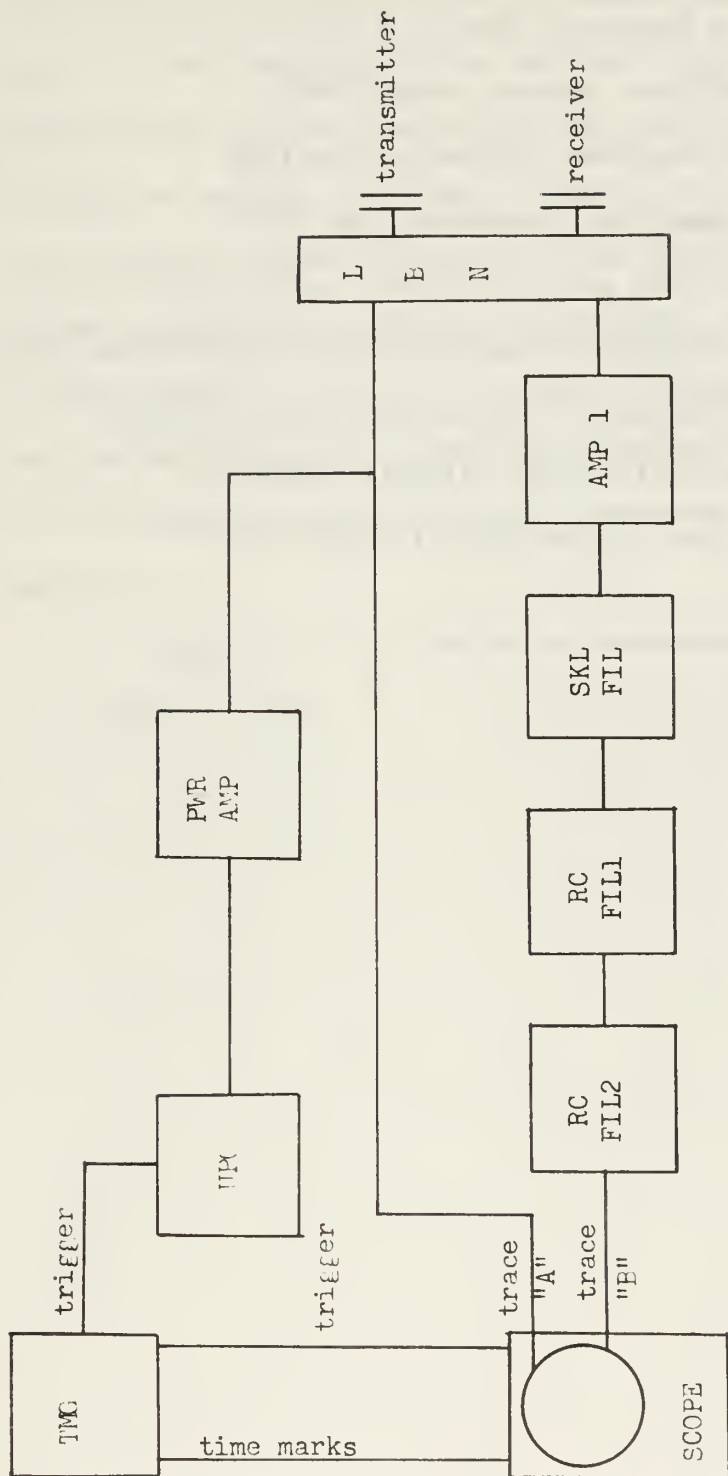
The pressure-sensitive barium titanate was constructed using eight 1/8 inch by 1/8 inch cylinders mounted on several strands of twisted wire, which provided the inner electrical connection. To provide the damping necessary to reduce the effect of longitudinal resonances, the spaces between the cylinders were filled with strips of rubber. The outer electrical connection was provided by a wire which was coiled around each cylinder. This probe proved to be somewhat insensitive and was used only for comparison purposes.

When the electrical load on the Mylar receiver (see Fig. 2.5) was terminated by the 1 megohm impedance of the voltage amplifier, the receiver was sensitive to particle displacement. Therefore, the Mylar receivers were used to measure the particle displacement, and the barium titanate array was used to measure the acoustic pressure. Transmitters and receivers are shown in Fig. 3.2.

Electronic Equipment

Figure 3.3 shows the block diagram of the equipment; Table 3.1 identifies the components in the figure. The unit-pulse generator was used for the step input.

The received signal was sent from the receiver through the load and bias network, amplifier and filters to trace "B" of the dual-beam oscilloscope. The output of the power amplifier could be displayed on trace "A". Measurements of the received waveform axis crossings and amplitudes were made directly from the oscilloscope display, or photographed for later analysis. The electronics were triggered by the time-mark generator which also triggered the time-base of the oscilloscope. The intensity of the "B" trace was modulated by a 10 usec marker available from the time-mark generator.



Block diagram of electronics equipment, identified in Table 3.1.

Figure 3.3

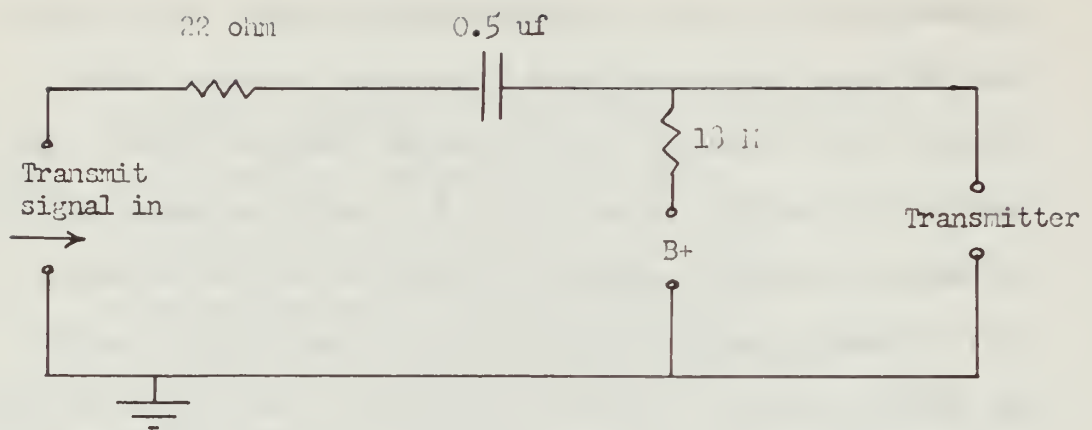
Table 3.1

Electronics Equipment

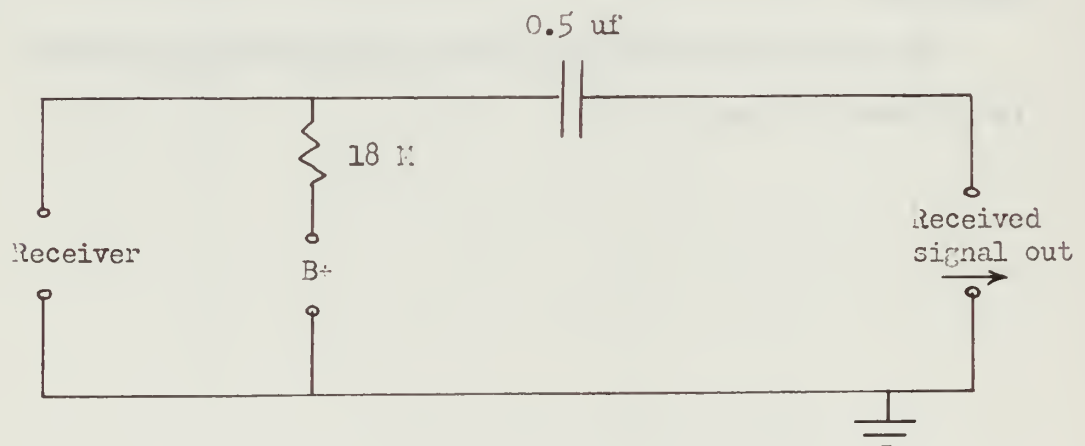
UPG	Unit pulse generator, General Radio type 1217-B
PWR AMP	Power amplifier, Hewlett Packard 467-A
TMG	Time Mark Generator, Tektronic type 180A
AMP 1	Voltage amplifier, Tektronic type 1121A
SKL FIL	Electronic band pass filter, SKL model 202-D
RC FIL1	Homemade variable low-pass RC filter with 400 khz roll-over
RC FIL2	Homemade high-pass RC filter with 2 khz roll-over
SCOPE	Dual beam oscilloscope, Fairchild model 777
LBN	Load and bias network shown in Fig. 3.4.

Source and receiver were carefully positioned so that the distance between adjacent sides, r-a, was always the same. This insured that the trace modulation would be properly positioned with respect to the inception of the received transient signal. The load and bias network shown in Fig. 3.4 served to supply the D.C. voltage bias needed by the Mylar transducers without allowing this voltage to appear elsewhere in the circuit and to provide the proper electrical load for the receiver. The 22 ohm resistor in the transmitter circuit was needed to suppress parasitic oscillations caused by the transient excitation of the capacitance of the transmitter and the residual inductance of the power amplifier.

The rise time of the system was experimentally determined to be about 0.5 usec.



Transmitter Bias Network



Receiver Bias Network

Load and bias network

Figure 3.4

4. EXPERIMENTAL INVESTIGATION

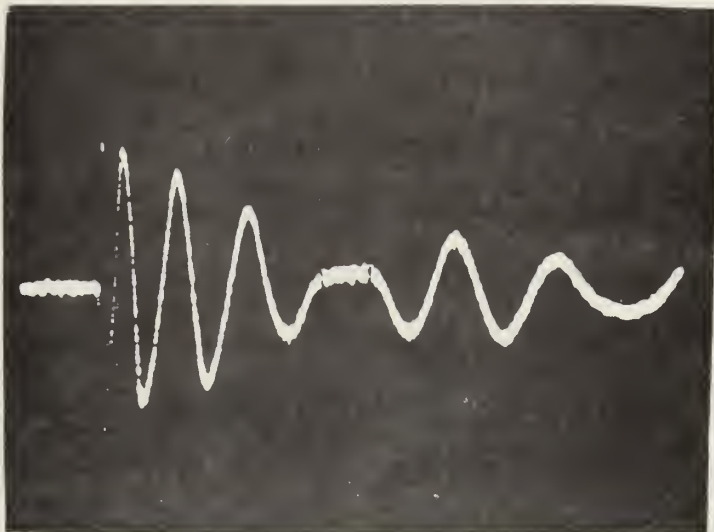
The purposes of the experimental investigation were to (a) observe and analyze the received acoustic pressure and radial particle displacement waveforms in the layer, (b) compare these waveforms with the theoretical predicted waveforms produced by the computer programs, and (c) vary the value of the ratio N/N_a over a large range to investigate the validity of the assumed asymptotic approximations previously discussed. Four basic parameters characterized each experiment: the range r , the transmitter radius a , the layer depth d , and the speed of sound, c .

Experimental Procedures

Before each run, it was decided which parameter would be varied. Generally, the time of flight T and the depth of the layer d were kept constant while the source radius a was varied throughout its range. The 0.25 cm radius Mylar transducer was used to record the received particle displacement, and the barium titanate linear array was used for the acoustic pressure receiver. The temperature of the water was measured to determine the speed of sound in the layer⁽¹⁷⁾. The depth was determined by averaging several physical measurements taken over the ensonified area. Another method of determining the depth was to excite the tank as a pressure-release cavity. The cut-off frequency could then be determined by observing the received signal on an oscilloscope and varying the frequency until the signal disappeared. Once the cut-off frequency was known, the depth could be calculated, using the formula $w_n = \frac{\pi c}{d}$. Because of the irregularities observed in the depth, this method proved to be no more accurate than the

actual measurement using a ruler and was consequently abandoned. The intensity of the trace of the oscilloscope was modulated by a 10 usec marker available from the time-mark generator. The source and receiver were carefully positioned so that the distance between adjacent sides, $r-a$, was always the same and such that the reception of the received transient and one of the time marks always coincided. This insured that when changing transmitters, identical positioning and time of flight could be achieved.

The received waveforms were photographed from the oscilloscope display. For the step input, several photographs were taken of each waveform. An expanded time scale was used when photographing the leading portion of the waveform which contained the high frequencies. For a typical experimental run, three photographs of each waveform were made utilizing, for example, 20 usec/cm time scale. By varying the delay time vernier, the entire waveform could be displayed and photographed for later analysis. By careful measurement of the position of each axis crossing with the neighboring time marks, the relative phase of each axis crossing could be compared between the photographs taken for different source radii. The amplitudes of the peaks of the waveforms were read with the help of dividers and a scale. Sample photographs are shown in Fig. 4.1. It should be noted that the anomalous behavior of the received waveforms as evidenced by Fig. 4.1 departs drastically from the smoothly-varying computer predictions of Figs. 2.1 and 2.2. This anomaly will be discussed in more detail later.



Step Input
in Velocity

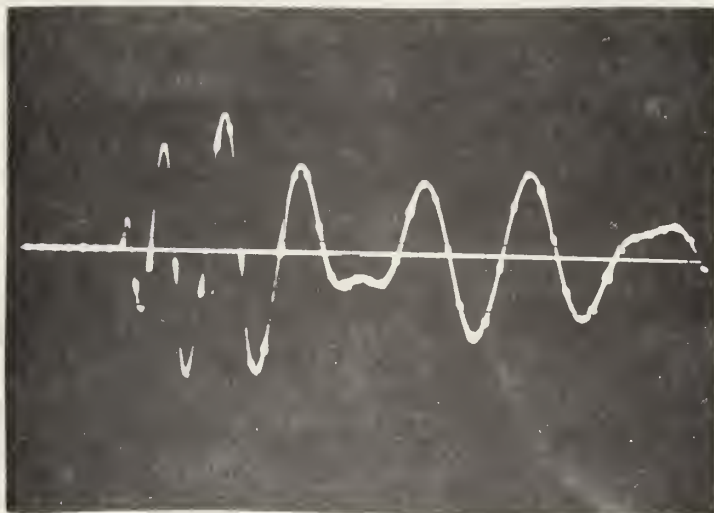
$r=63.0$ cm

$a=6.00$ cm

$d=8.00$ cm

temp= 22°C

(a) Received Acoustic Pressure



Step Input
in Velocity

$r=91.4$ cm

$a=6.00$ cm

$d=8.00$ cm

temp= 16.5°C

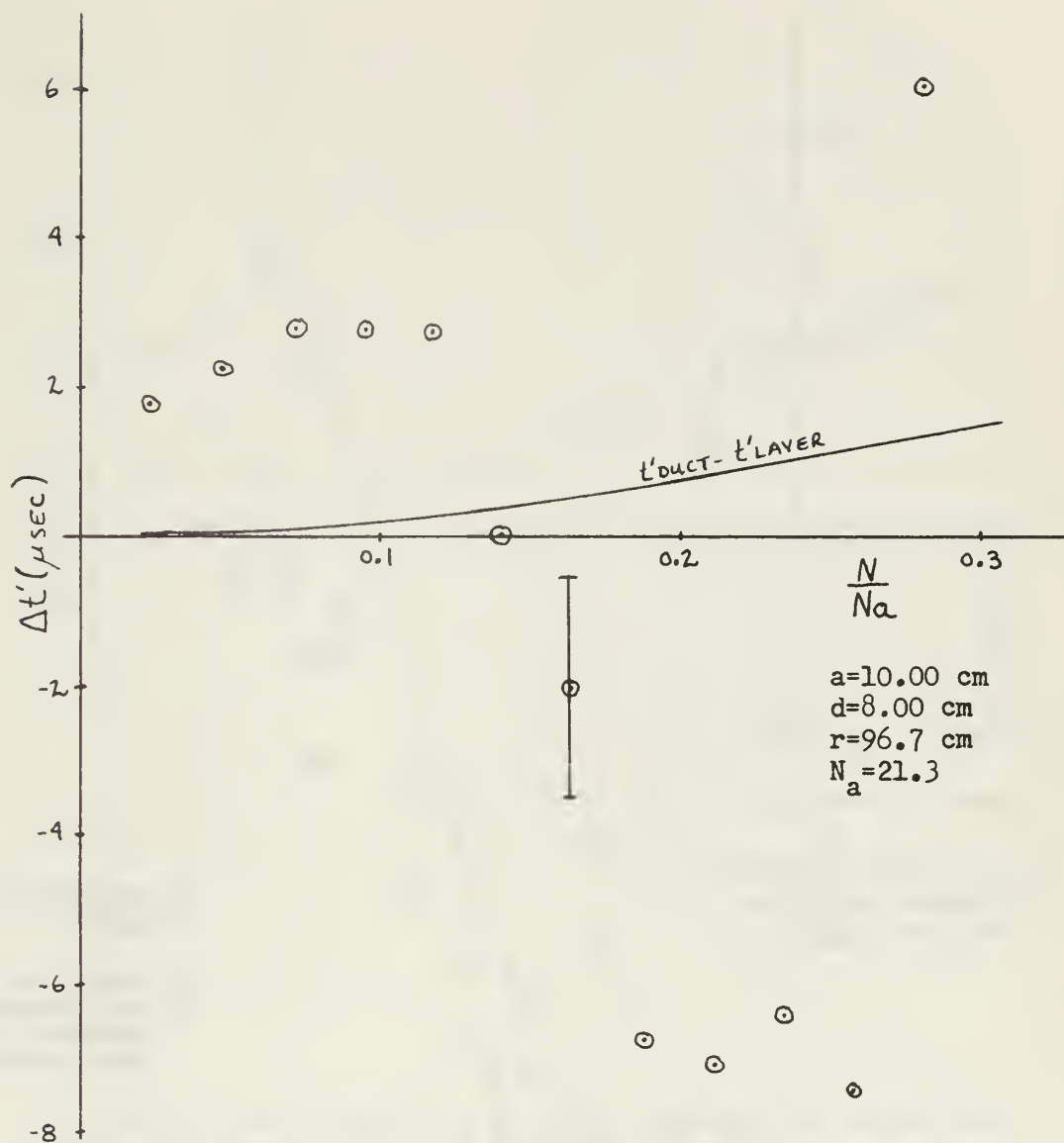
(b) Received Particle Displacement

Observed Waveforms

Figure 4.

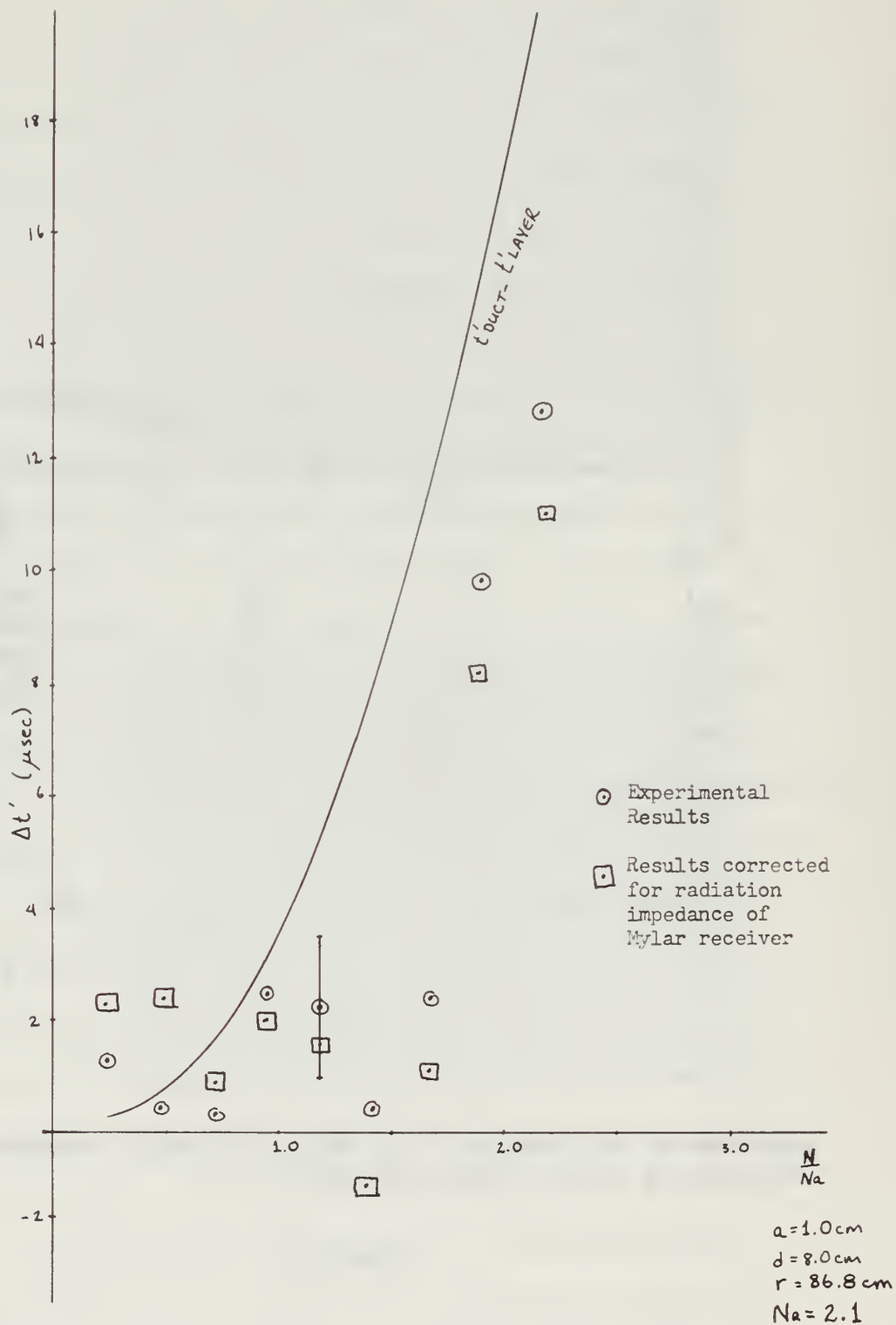
For each experimental run, a corresponding computer run was made using the same values for r , a , c , and d . The computer programs were written so that their output for each run included graphs of the predicted waveforms, times of axis crossings for the layer solution t'_m and for the duct solution t'_{om} , and amplitudes of the peaks and the time of occurrence of these peaks for the layer solution. In this manner, the theoretical values of the times of axis crossings and of the amplitude peaks could be compared with those values experimentally determined.

The time of the axis crossings were compared in the following manner: Previous work⁽⁵⁾ suggested that the time of each axis crossing should be the same as the theoretically predicted t'_m within the validity of the approximations used. As was shown in section 2, the theory was valid only as long as $N/N_a \leq 1$. Therefore, the convenient parameters for analyses were the time of the axis crossings and the ratio N/N_a . In order to reduce the size of the graphs, the time coordinate was reduced by the amount t'_m predicted by the computer. The time coordinate signified by $\Delta t'$ was plotted against the ratio N/N_a . Figures 4.2 to 4.4 are representative examples of these graphs. The solid line represents the values of $t'_{om} - t'_m$, and the circled dots represent the values of $t'_{exp} - t'_m$. Were the theory to have been completely correct and the experiment accurate enough, the data would have fallen on the X-axis (which represents $t'_m - t'_m$). As can be seen from Figs. 4.2 to 4.4, the data were not in agreement with the theory. The effect of the phase angle demonstrated in Fig. 2.6 was taken into account and



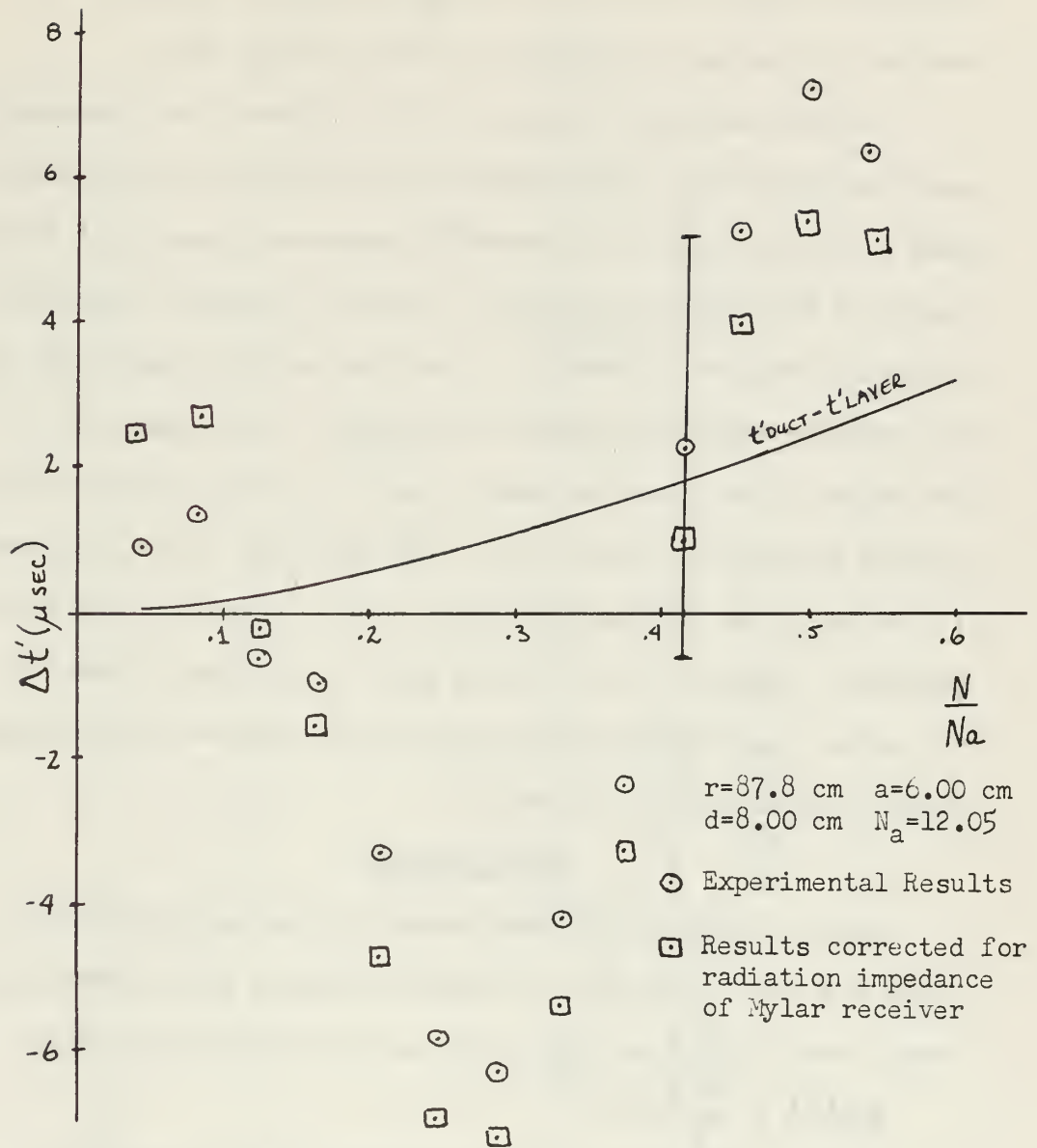
Experimental and Computed t' vs. N/N_a for Acoustic Pressure Waveform Generated by a Step Input in Velocity^a.

Figure 4.2



Experimental and Computed t'_m vs. N/N_a for Particle Displacement Waveform Generated by a Step Input in Velocity for $a = 1.0 \text{ cm}$.

Figure 4.3



Experimental and Computed t'_m vs. N/N_a for Particle Displacement Waveform Generated by a Step Input in Velocity for $a = 6.0 \text{ cm}$.

Figure 4.4

plotted on Figs. 4.3 and 4.4. As can be seen, this did not improve the agreement between the theory and the data.

The peak-amplitude data were also analyzed. The experimental amplitude peaks were first normalized to the value of the highest peak in the waveform. The predicted peaks were normalized in the course of the computer programs. The ratio of these normalized quantities was then plotted as a function of the delayed time of the predicted amplitude peaks for each run. Exact agreement in the shape of the transient would result in a line of zero slope passing through the point (1,0). The amplitude effect discussed in Section 2 for a Mylar transducer used as a receiver was also plotted. Figures 4.5 to 4.7 show plots for various values of r , a , and d . Once again, this effect did not improve the agreement between the theory and the data.

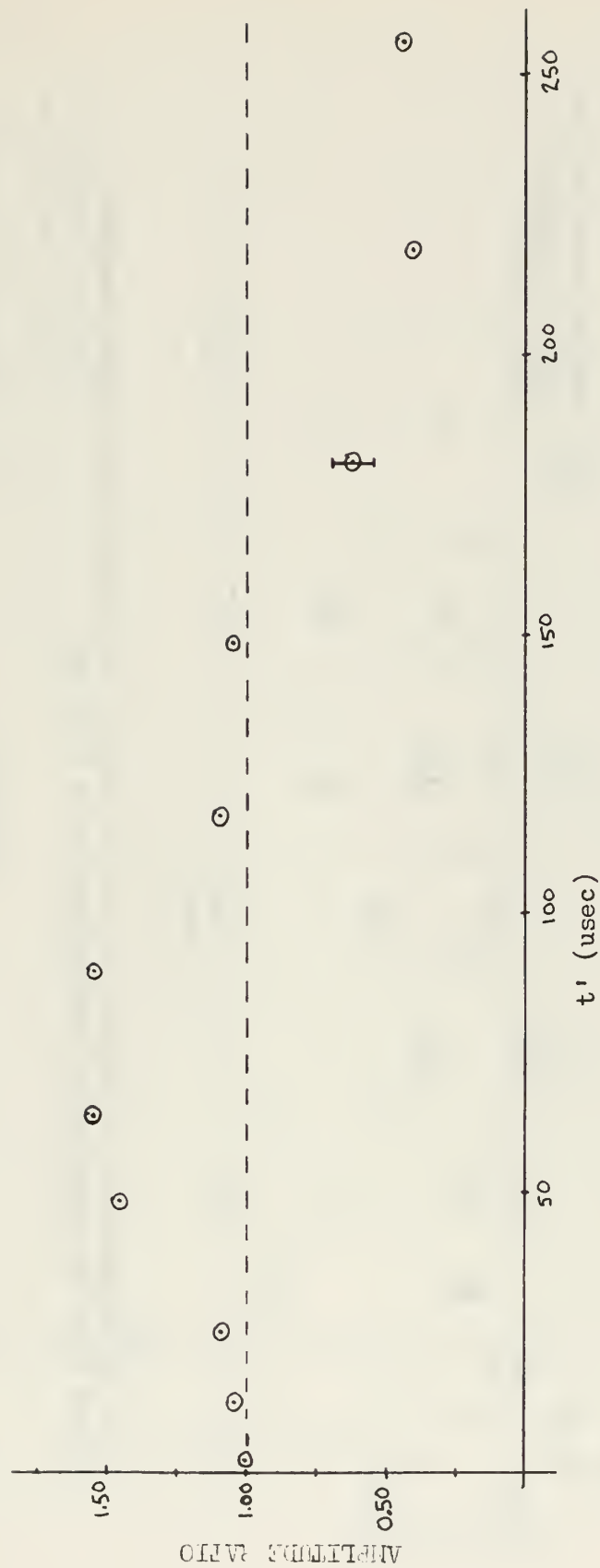
Error Analysis

The rise time of the experimental system was determined to be about 0.5 usec. Therefore, instead of being a perfect step-function input, the velocity at the source was initially described by

$$V_a(t) = 1 - e^{-\alpha t}$$

where $\alpha = 2 \times 10^6 \text{ sec}^{-1}$ is the reciprocal of the rise time.

Previous work⁽⁵⁾ has indicated that the rise time of the system should introduce distortion into the received signal for at most 3.0 usec of delayed time t' . Since this time is less than that for the first maxima, the effect of the rise time on the received signal can be ignored in this investigation.



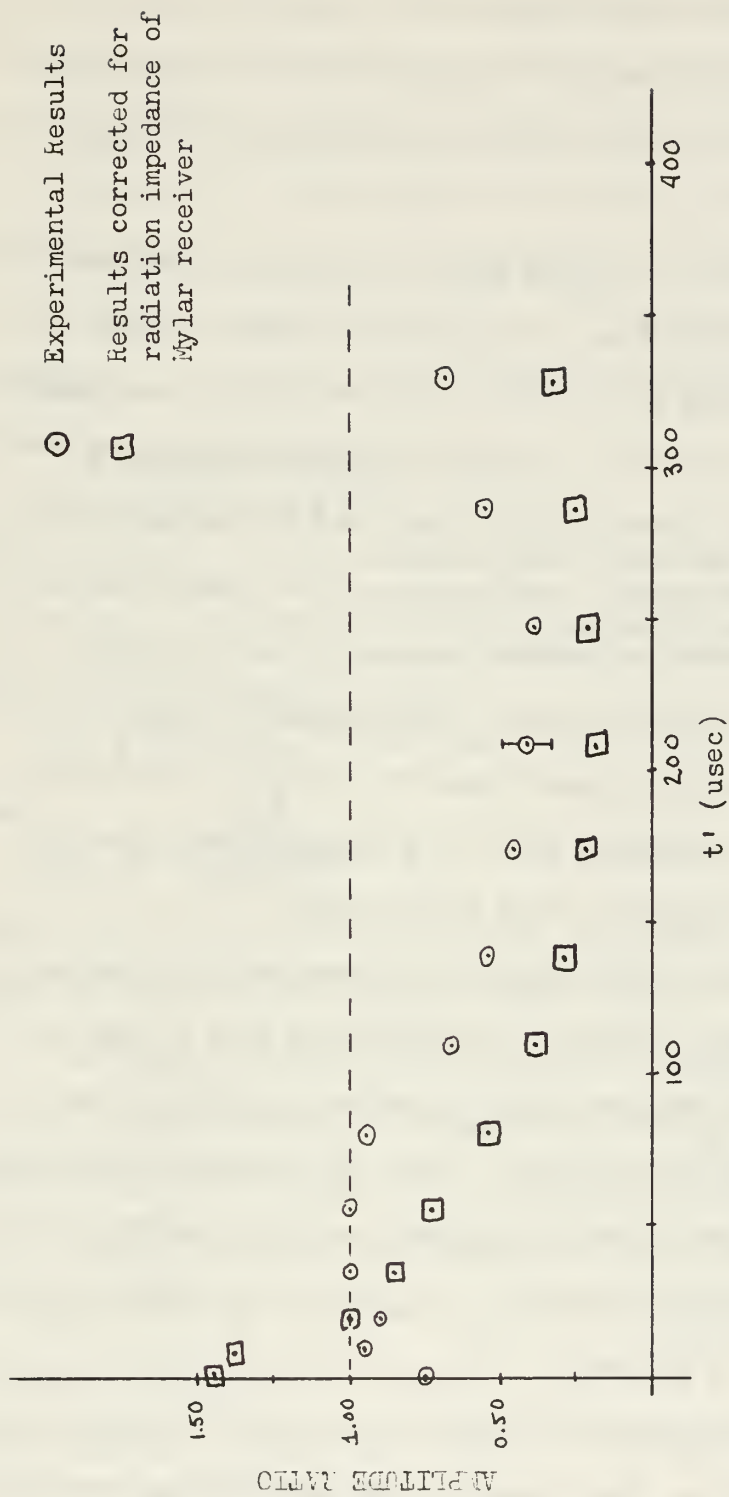
Ratio of Experimental to Computed Normalized Acoustic Pressure Amplitudes Generated by a Step Input in Velocity vs. Delayed Time.

Figure 4.5



Ratio of Experimental to Computed Normalized Particle Displacement Amplitudes Generated by a Step Input in Velocity vs. Delayed Time for $a = 1.0$ cm.

Figure 4.6



Ratio of Experimental to Computed Normalized Particle Displacement Amplitudes Generated by a Step Input in Velocity vs. Delayed Time for $a = 6.0$ cm.

Figure 4.7

It has been shown that the velocity of the Mylar face decays to 88 per cent of its maximum value after a time of 360 usec⁽⁵⁾. This effect is not large enough to account for the tailing off of the amplitude peaks of the received waveforms seen in Figs. 4.5 to 4.7.

Uncertainties in r , a , c , and d were the possible sources of error in this investigation. The effective radius of each transmitter was measured to the nearest 0.5 mm, which could have introduced an uncertainty of ± 1.0 per cent in the value of a for the 6.0 cm radius source and ± 5.0 per cent in the value of a for the 1.0 cm radius source. Measurement of the temperature of the water to the nearest half-degree restricted the systematic error in c to within ± 0.5 per cent. Determination of the time-of-flight T of the received signal from the source to the receiver produced a possible systematic error of ± 0.5 per cent, which in turn resulted in an error in r of ± 0.5 per cent.

The largest experimental error was encountered in determining the depth of the layer. Observed irregularities of ± 1.0 mm in the bottom surface of the tank could introduce an error in the local effective depth of the layer. Since the averaged layer depth used as an input to the computer programs was only accurate to ± 1.0 mm, the systematic error introduced in w_n was on the order of ± 3.0 per cent for a depth of 8.0 cm.

The error in determining the times of the axis crossings from the data was effected by the accuracy of the oscilloscope time-base which was calibrated to within 0.3 per cent. With the trace of

the oscilloscope modulated with the 10 usec marker as an additional time reference, this error was reduced even more. Therefore, a random error of ± 1.0 per cent could be expected when one takes into account the accuracy of reading the oscilloscope scale.

The errors in the computed values of t'_m were influenced predominately by the error in w_n , since it appears in the argument of the Bessel functions ($w_n \sqrt{t'^2 - T^2}$) from which the t'_m are computed. It has been shown⁽⁵⁾ that the argument of the Bessel functions could be rewritten as

$$w_n \sqrt{t'_m(t'_m + 2T)} = C_m$$

where C_m are a set of constants which yield zero values for the amplitude of the particle-displacement solution. For the leading portion of the signal, we have

$$w_n \sqrt{2T} (t'_m)^{1/2} \approx C_m$$

and

$$t'_m \approx \frac{C_m^2}{w_n^2 2T}.$$

Therefore, the ± 3.0 per cent error in w_n could lead to a ± 6.0 per cent error in the computed values of t'_m .

To reduce the scatter of the data, a one-parameter fit was tried. It was decided to determine an effective cut-off frequency and use this as an input to the computer programs instead of the layer depth. This was accomplished by determining the cut-off frequency for the values of t'_{exp} and the arguments of the trig function approximations developed in Section 2. At an axis crossing, the argument was equal to an integer multiple of π

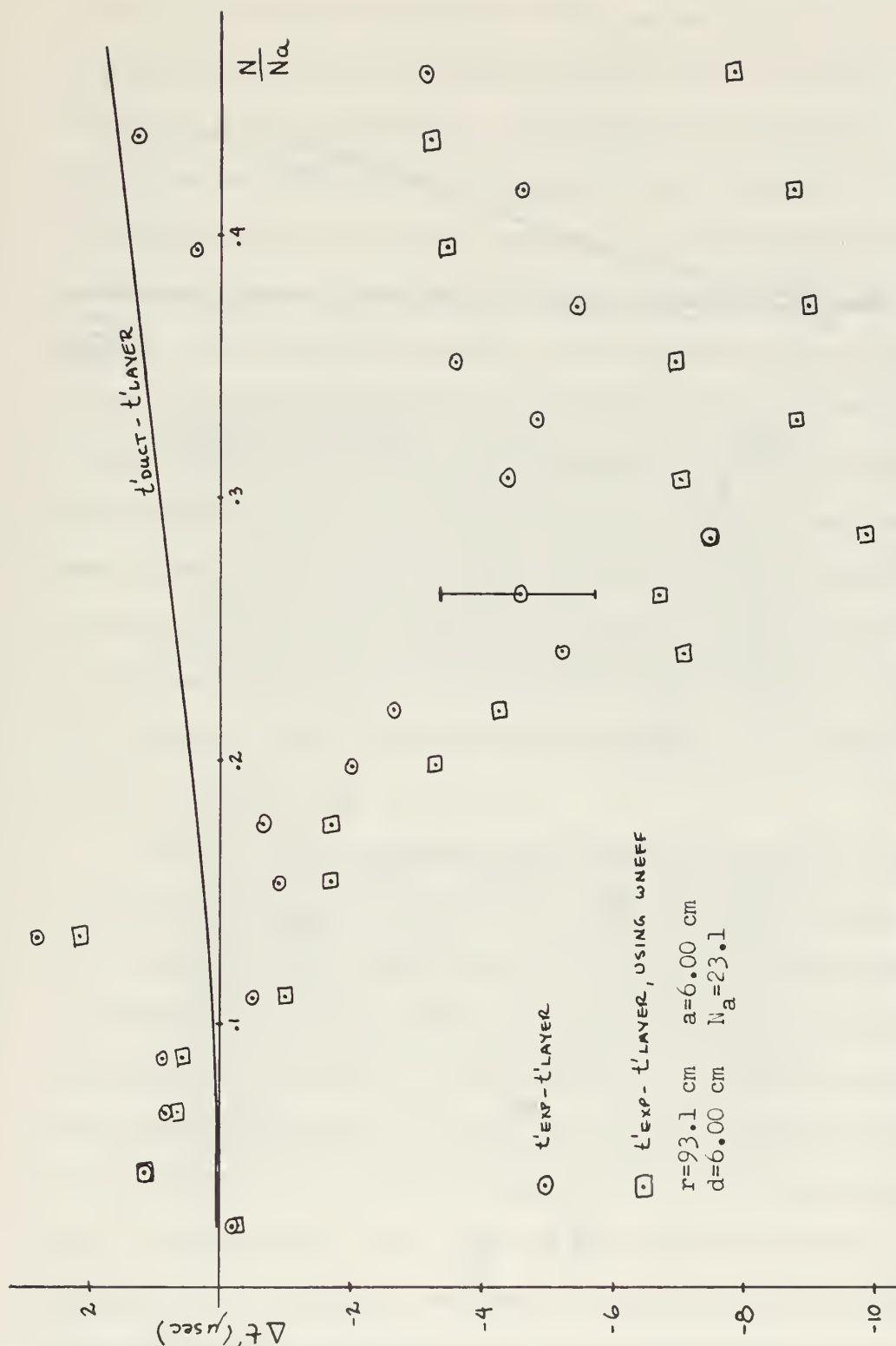
$$\left[w_n \sqrt{t'_{\text{exp}}(t'_{\text{exp}} + 2T)} - \frac{\pi}{4} + \delta \right] = m\pi.$$

A computer program was written to evaluate the cut-off frequency for each axis crossing. Then, these cut-off frequencies were averaged to give an "effective cut-off frequency" to be used in the computer programs to recompute the time for each axis crossing. Figure 4.8 shows the effect of this one-parameter fit. As can be seen, it did not improve the scattering significantly and was not used.

Error flags on Figs. 4.2 to 4.8 indicate the relative magnitudes of errors in the experimental and computed values of the axis crossings and peak amplitudes. However, these error flags are not large enough to explain the scatter of the data or the anomaly which was present (see Fig. 4.1). The theory could not account for this anomaly so various experiments were conducted to investigate its character and source of origin.

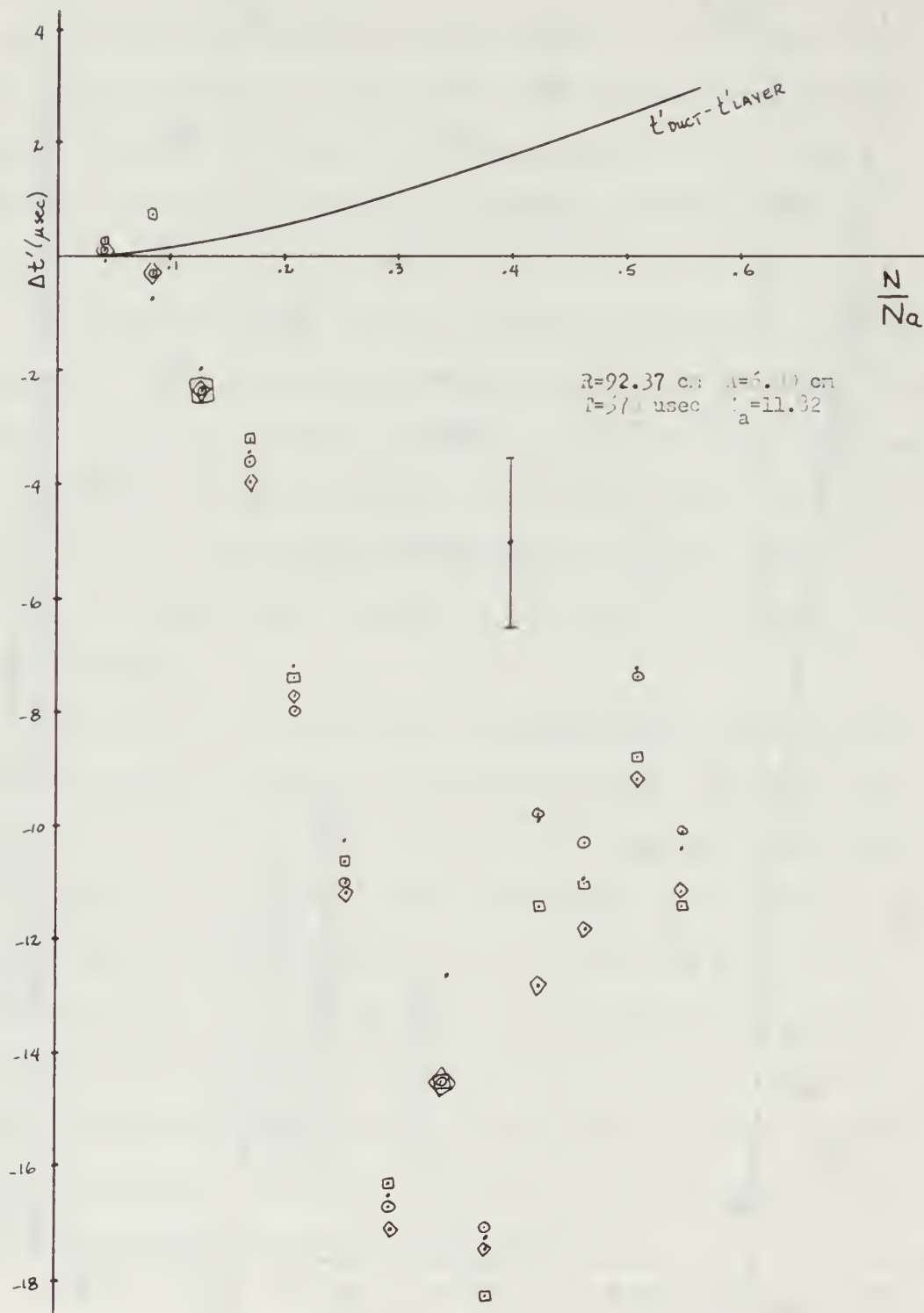
Firstly, it was suggested that irregularities in the bottom of the tank might be a possible cause of the anomaly. Therefore, the relative positions of the transmitter and the receiver in the tank were changed. The values of T and d were always kept constant. Four contrasting positions were chosen; one near the left hand side of the tank, one in the center of the tank, one adjacent to a seam in the bottom near the right hand side, and one where the transmitter and receiver straddled the seam. As can be seen in Fig. 4.9, within the experimental accuracy of the investigation, positioning on the bottom had no effect on the received waveform.

Secondly, it was decided to monitor the current drawn by the transmitter when loaded by the water medium and compare this with the current predicted assuming ρ_c loading. The current was



Experimental and Computed t'_m vs. N/N_a for Particle Displacement Waveform Generated by a Step Input in Velocity using a One Parameter Fit.

Figure 4.8

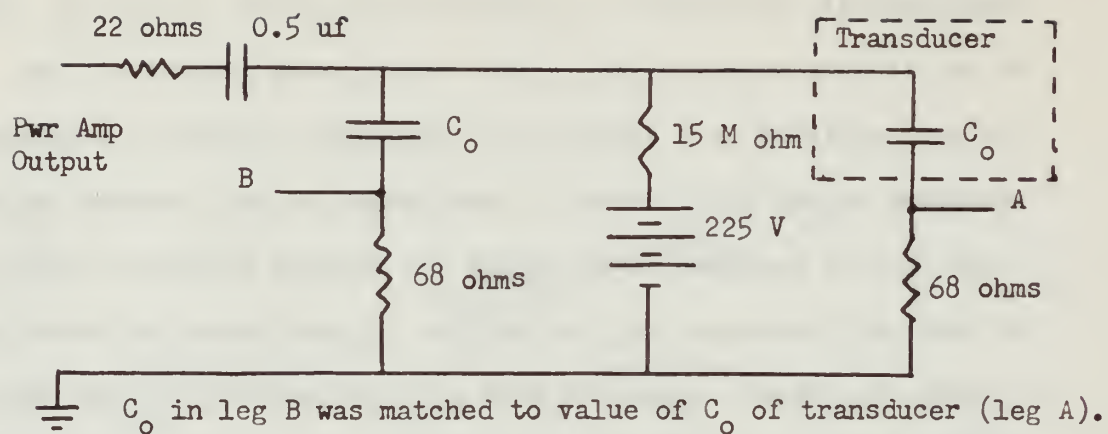


Experimental and Computed t_{IN} vs. N/N_q for Particle Displacement Waveform Generated by a Step Input in Velocity^a for Four Positions on the Tank Bottom.

Figure 4.9

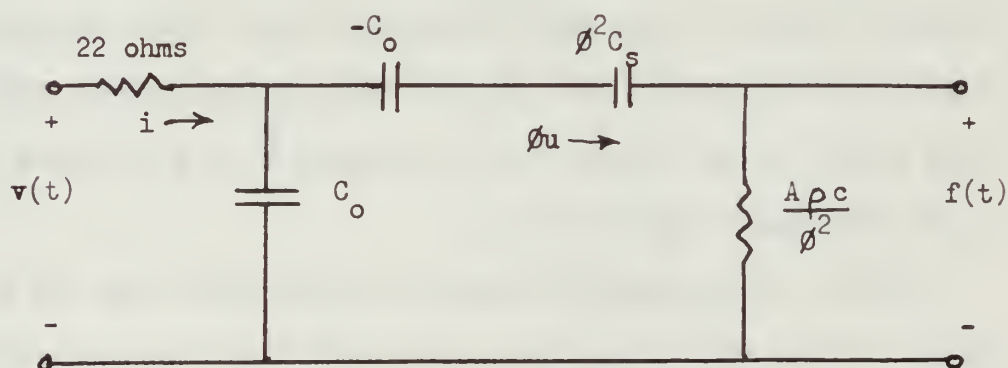
experimentally determined by measuring the current in the two legs of the circuit shown in Fig. 4.10. The current present in each leg was amplified by a differential amplifier and then the difference displayed on the oscilloscope. Photographs of the received signal could then be analyzed to determine the current drawn as a result of acoustic radiation into the medium. By analyzing the equivalent circuit of a Mylar transducer used as a transmitter⁽¹⁶⁾, as shown in Fig. 4.11, the predicted value of the current drawn as the result of the assumed ρc loading can be determined. For this assumed loading, the current drawn by the mechanical leg of the source should be flat. Typical values for the 6 cm radius source were near 6 uamp. The measured values of the current had rapid oscillations of nearly 1 uamp peak-to-peak amplitude, which indicated a significant fluctuation from the flat response predicted. This casts doubts on the validity of the assumption of ρc loading used in the developments of Section 2.

Lastly, it was suggested that the polyethylene foam was not a perfect pressure-release surface and that transmission through it into the wood bottom was the cause of the anomaly. In order to investigate this possibility, two additional layers of polyethylene were glued to the bottom of half the tank. Then runs were made on the single-layered bottom and then on the three-layered bottom. The quantities r , a , and d were kept constant for the corresponding runs. Figures 4.12 to 4.14 indicate the predicted waveform, the experimentally determined waveform on the three-layered bottom, and the experimentally determined waveform on the single-layered bottom for three values of a : 10, 6, and 4 cm. The vertical and horizontal



Circuit used to Monitor Current Drawn by a Mylar Transducer as a Result of Acoustic Radiation into a Water Medium.

Figure 4.10



$$C_o = .018 \text{ uf}$$

$$A = 3.02 \times 10^{-2} \text{ m}^2$$

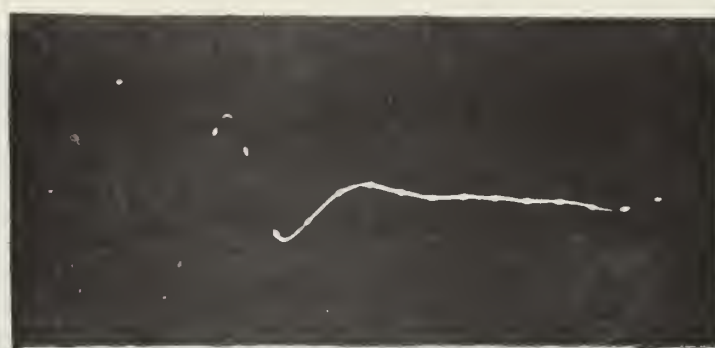
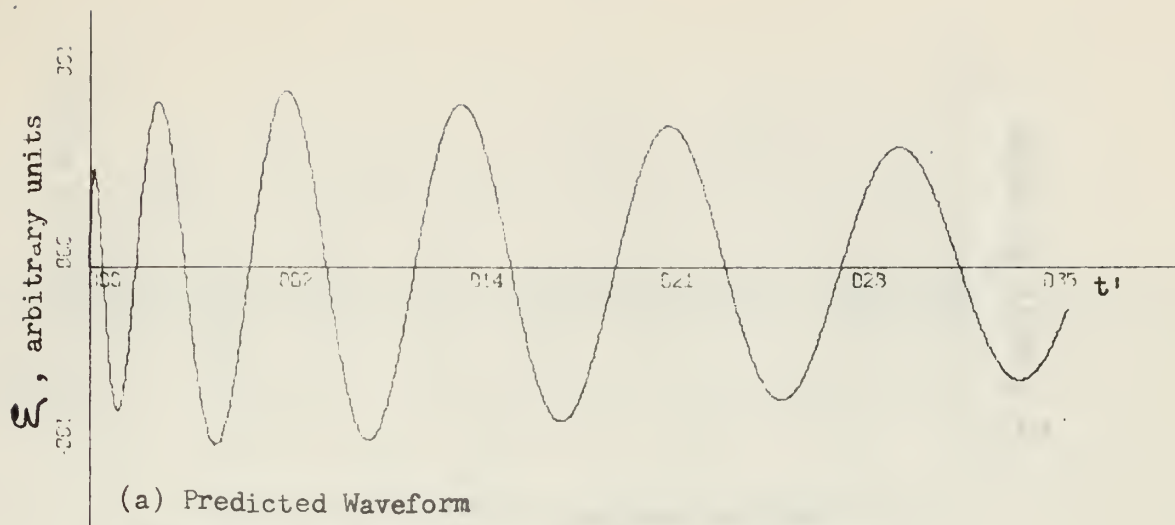
$$C_s = 10^{-6} \text{ m/N}$$

$$\phi = 0.1 \text{ N/volt}$$

$$\rho c = 1.5 \times 10^6 \text{ kg/sec-m}^2 \quad v(t) = 20 \text{ volt step input}$$

Equivalent Circuit of a Mylar Transducer used as a Transmitter.

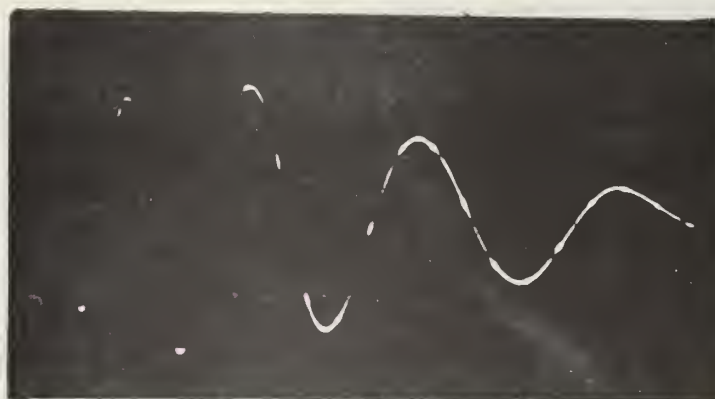
Figure 4.11



Step Input
in Velocity

$r=70.66$ cm
 $a=10.00$ cm
 $d=8.00$ cm

(b) Received particle displacement waveform on three-layered bottom



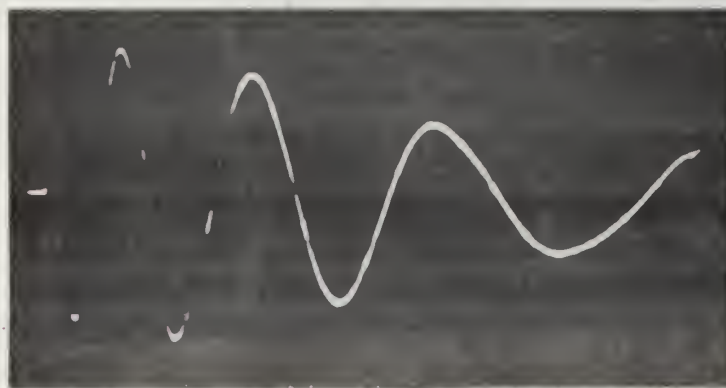
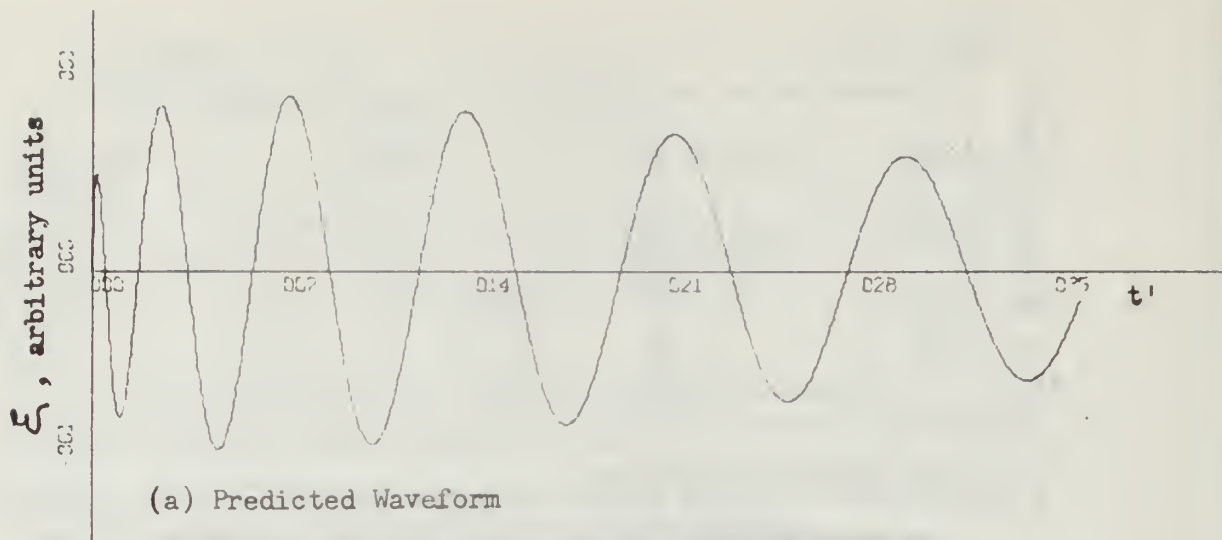
Step Input
in Velocity

$r=70.66$ cm
 $a=10.00$ cm
 $d=8.00$ cm

(c) Received particle displacement waveform on single-layered bottom

Bottom Layer Investigation for Three-Layered Bottom and Single-Layered Bottom using 10.00 cm Source.

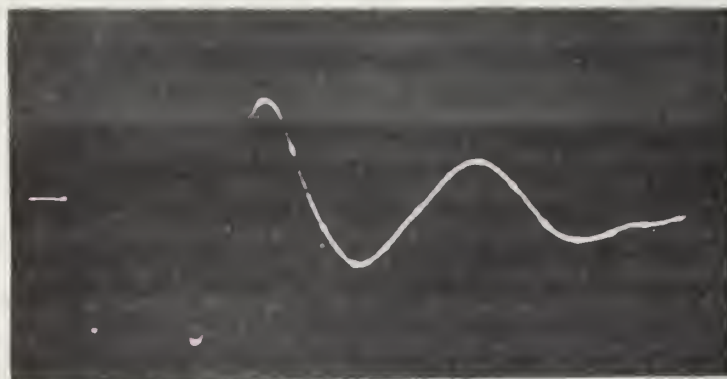
Figure 4.12



Step Input
in Velocity

$r=66.66$ cm
 $a=6.00$ cm
 $d=8.00$ cm

(b) Received particle displacement waveform on three-layered bottom



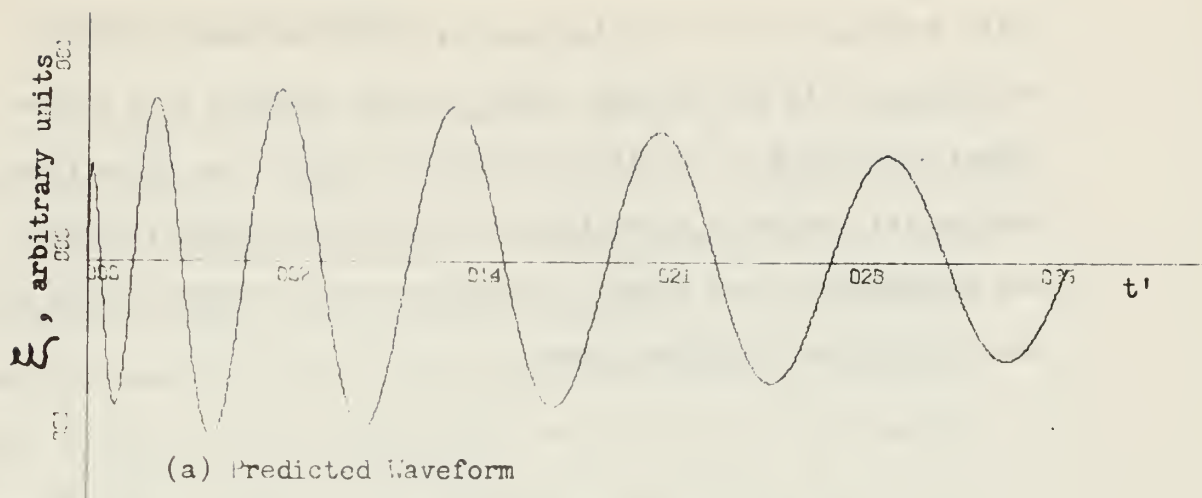
Step Input
in Velocity

$r=66.66$ cm
 $a=6.00$ cm
 $d=8.00$ cm

(c) Received particle displacement waveform on single-layered bottom

Bottom Layer Investigation for Three-Layered Bottom and Single-Layered Bottom using 6.00 cm Source.

Figure 4.13



Step Input
in Velocity

$r=64.66$ cm
 $a=4.00$ cm
 $d=8.00$ cm

(b) Received particle displacement waveform on three-layered bottom



Step Input
in Velocity

$r=64.66$ cm
 $a=4.00$ cm
 $d=8.00$ cm

(c) Received particle displacement waveform on single-layered bottom

Bottom Layer Investigation for Three-Layered Bottom and Single-Layered Bottom using 4.00 cm Source.

Figure 4.14

scale settings on the oscilloscope were kept the same for each set of runs. As can be seen, there is some evidence of a bottom effect, but there is no clear correlation between the three runs. However, this evidence is sufficient to doubt the credibility of the assumption of the perfect pressure-release characteristics of the 0.25 inch polyethylene foam.

5. RESULTS AND CONCLUSIONS

The investigation has shown that for $N/N_a \leq 1$ the predicted and experimentally observed shifts in axis crossings should agree to within ± 6 per cent if one takes into account just the known systematic errors. The correlation between the predicted and observed amplitudes should be of the same accuracy. However, the difference between the theory and data is greater than that expected.

The theory as developed in Section 2 could not account for the anomaly which was present in all runs, but the qualitative agreement between the observed and predicted waveforms and the general agreement with the solutions developed in other work^(4,5,10,13) lead one to believe that the theory presented in Section 2 is correct.

It is concluded that the experimental setup used is not accurate enough to give results needed to confirm the theory.

It is recommended that better electronic equipment and transducers should be investigated. Further studies should be conducted to check the validity of the assumed pressure-release characteristics of the polyethylene foam. More investigations are needed to try to determine the cause of the observed anomaly.

BIBLIOGRAPHY

1. D. V. Anderson and C. Barnes, J. Acoust. Soc. Am. 25, 525-528 (1953).
2. J. M. Proud, P. T. Tamarakin and E. T. Kornhauser, J. Acoust. Soc. Am. 28, 80-85 (1956).
3. K. Walther, J. Acoust. Soc. Am. 33, 681-686 (1961).
4. A. B. Coppens, J. Acoust. Soc. Am. 40, 331-341 (1966).
5. A. C. Miller and G. F. Wendt, Propagation of Two Simple Acoustic Transients in an Isovelocity Layer with Perfectly-Reflecting Boundaries, Thesis, Naval Postgraduate School, Monterey, California (1967).
6. W. C. Knudsen, J. Acoust. Soc. Am. 29, 918-924 (1957).
7. L. M. Brekhovskikh, Waves in Layered Media, trans. D. Lieberman. (Academic Press, New York, 1960), Chap. 5.
8. J. R. Wait, J. Res. Natl. Bur. Std. (U.S.), 69D, 1287-1401 (1965).
9. J. W. Miles, J. Acoust. Soc. Am. 25, 1087-1089 (1953).
10. R. G. Barakat, J. Acoust. Soc. Am. 33, 1759-1764 (1961).
11. C. M. Knop, IEEE Trans. on Antennas and Propagation AP12, 494-496 (1964).
12. C. T. Case and R. E. Haskell, IEEE Trans. on Antennas and Propagation AP12, 401 (1966).
13. R. E. Haskell and C. T. Case, IEEE Trans. on Antennas and Propagation AP15, 458-464 (1967).
14. A. B. Coppens, private communication.
15. U. S. Department of Commerce, Handbook of Mathematical Functions, ed. M. Abramowitz and I. Stegun, (U.S. Government Printing Office, Washington, D. C., June 1964), Chap. 9.
16. G. L. Palatini, Electroacoustic Properties of Mylar Dielectric Underwater Sound Transducers, Thesis, Naval Postgraduate School, Monterey, California (1966).
17. M. Greenspan and C. E. Tschiegg, J. Acoust. Soc. Am. 31, 75-76 (1959).

* * * * *

APPENDIX A

PROGRAM STEP1

THIS PROGRAM GIVES GRAPHS OF THE ACOUSTIC PRESSURE(PNRAT) AT A METERS POSITION (R-A) METERS FROM A CYLINDRICAL SOURCE OF RADIUS,A, METERS IN A PRESSURE RELEASE ISO-VELOCITY LAYER OF DEPTH,D,METERS AS A RESULT OF A STEP INPUT IN VELOCITY AT R-A=, AT TIME,T,=.

THESE ACOUSTIC VARIABLES ARE OBTAINED BY EVALUATING COMBINATIONS OF TRUNCATED INFINITE SUMS OF BESSEL FUNCTIONS. PNRAT CONSISTS OF A MAIN DUCT SOLUTION TERM,PMAIN, AND A CORRECTION TERM,PNCOR, FOR THE LAYER. PNRAT IS GRAPHED TO SHOW THE FULL SOLUTION FOR THE LAYER. AXIS CROSSINGS FOR PNRAT AND PMAIN ARE CALCULATED. THE MAXIMA(+ OR -) OF PNRAT (PNRATM) AND THE DELAYED TIME OF THESE MAXIMA (TPRIM) ARE DETERMINED.

INPUT DATA

DATA FIELDS

ALL FIELDS

DATA DESCRIPTION (ALL MKS UNITS)

- R=DISTANCE FROM RECEIVER TO CENTER OF TRANSMITTER
- A=RADIUS OF SOURCE
- DELT=INCREMENT OF TIME BY WHICH VALUES ARE GENERATED.
- TPMAX=MAXIMUM DELAYED TIME FOR WHICH VALUES ARE GENERATED.
- C=SPEED OF SOUND IN LAYER.
- FN= NORMAL MODE NUMBER OF THE LAYER CONTRIBUTING TO VALUES.
- D=DEPTH OF WATER IN LAYER.
- I3,7X,7E11,:(8E11,):) FOR MAT FOR EXPERIMENTAL DATA. I3 IS FORMAT FOR N1 AND N2 EXPLAINED BELOW. 7X SKIPS TO COLUMN 11 AND REMAINING FIELDS,ALL E10.0, ON AS MANY CARDS AS ARE NEEDED FOR EXPERIMENTAL DATA.
- N1=NUMBER OF EXPERIMENTAL AXIS CROSSINGS IN PRESSURE.
- ACXP=EXPERIMENTALLY DETERMINED AXIS CROSSINGS IN PRESSURE.
- N2=NUMBER OF EXPERIMENTAL MAXIMA (+ OR -) IN PRESSURE.

AMPXP=EXPERIMENTALLY DETERMINED VALUES OF PEAK
AMPLITUDES (+ OR -) IN PRESSURE.

OTHER VALUES

CPT= TIME OF FLIGHT OF SOUND FROM SOURCE TO RECEIVER AT POSITION R
WN=CUT-OFF FREQUENCY OF MODE NUMBER EN
TPRI=DELAYED TIME. THE TIME WHICH HAS ELAPSED AT A POSITION R SINCE
THE TRANSIENT FIRST REACHED THAT POINT. TPRI WILL RUN FROM 0 TO
TPMAX.
S= DUMMY QUANTITY FOR CALL RES SUBROUTINE.
ARG=ARGUMENT OF BESSEL FUNCTION.
TVAL=SQRT((T-CPT)/(1+CPT))
RESULT=VALUE RES SUBROUTINE GIVES IN CALCULATING PNPRAT.
ACOPM=COMPUTED AXIS CROSSING IN DUCT TERM,PNMAIN.
TPRIA=COMPUTED AXIS CROSSING IN PNPRAT.
CYCLEA=DELAYED TIME WHERE THEORY FAILS TO HOLD.
A MAXIMUM OF 999 POINTS WILL BE CALCULATED AND PLOTTED.

```

DIMENSION S(999),ARG(999),TPRI(999),TVAL(999),PNPRAT(999),
1PNCUR(999),PNMAIN(999),RESULT(999),ACOPR(39),PNRATM(39),TPRIM(39),
2ACXP(39),AMPXP(39),ACOPM(39)
3REAL(4)AREL/4H
REAL*8 ITITLE(12),STEPINI,,A,B,D,,ATES,PRI,XD,R,,
1,PNRAT,,VS,TPRI,,DELTE=.40,,S,TPMAX=,,367115,R=,
2,JJ=,
1 JK=J
ISIGN =
MAXCT =
READ(5,2)R,A,DELT,TPMAX,C,EN,D
FORMAT(7E17.5)
IF(DELT)200,200,201
200 STOP
CPT=(R-A)/C
DOVERA=D/A
WN=(3.1415927*EN*C)/D
CAWN=C/(A*WN)
TSURA=CPT*SQRT(1.+(1./CAWN)**2)
TPRIA=TSURA-CPT
CYCLEA=(WN*CPT)/(6.2831854*CAWN)
ACVERR=A/R
AC1=-.3./8.+(1./8.*ADOVER)

```

```

RCL=33./128. +G./128.*ANVERR + (9./128.)*ANVFR**2
CORR=2.*CAWN
FDGP = 1.0
I=1
TPRI(I)=0.0
3 TVAL(I)=SQRT(TPRI(I)/(TPRI(I)+2.*CPT))
ARG(I)=0.0
IF(TVAL(I) .NE. 0.0)ARG(I)=WN*TPRI(I)/TVAL(I)
* * * * *
3.1 THIS PORTION EVALUATES PNRT,PNMAIN,AND PNCOR FROM THE FOLLOWING
EXPRESSION,
(PNRT/(RHO*C))*(SQRT(R/A)/Z)=JSUB*(ARG)+A.1*CORR*F1 +R.1*CORR**2*
FDGP*F2 WHERE A.1=-(3/8 + 1/8*A/R)
R.1=33/128 + 6/128*A/R + 9/128*(A/R)**2
FDGP=2/3 CORR=2*CAWN AND CAWN=C/(A*WN)
F1=SUM(M=1 TO 10)((-1)**(M-1))*((T-CPT)/(T+CPT))*((2M-1)/2)*
JSUB(2M-1)(ARG)
F2=SUM(M=1 TO 10)((-1)**(M-1))*M*((T-CPT)/(T+CPT))*M*
JSUB(2M)(APG)
WHERE ARG=WN*SQRT(T**2-CPT**2)
JSUB(ARG)=PNMAIN AND REMAINDER =
PNCOR.
* * * * *
JC=21
TEMP=TVAL(I)
CALL RES(JC,ARG(I),RESULT(I),S)
4 PNMAIN(I)=S(1)
AXCRPM=PNMAIN(I)*PNMAIN(I-1)
IF(AXCRPM)41,42,42
41 JJ=JJ+1
ACOPM(JJ)=ARS(PNMAIN(I-1))/(ARS(PNMAIN(I-1))+ARS(PNMAIN(I)))
42 CONTINUE
SUM=TEMP*S(2)
TEMP2=TEMP**2
TEMPF2=TEMP*2
SUMF2=TEMPF2*S(3)
FM=1.0
DO 6 J=4,JC,2
TEMP = -TEMP*TEMP2
SUM=SUM+TEMP*S(J)
TEMPF2=-TEMPF2*TEMP2
FM=FM+1.0

```

```

6      SUMF2=SUMF2+FM*TEMPF2*S(J+1)
      CONTINUE
      PNCOR(I)=CORF*SUM*AC1 + B*1*FDGP*CORR**2*SUMF2
      PNRAT(I)=PNRAT(I)+PNRAT(I-1)
      IF(AXCRPP)6,1,6 2,6C2
6C1    KK=KK+1
      ACOPR(KK)=ABS(PNRAT(I-1))/(ABS(PNRAT(I-1))+ABS(PNRAT(I)))
      DELT+TPRI(I-1)
6J2    CONTINUE
      * * * * *
      THIS PORTION DETERMINES THE MAXIMA (+ OR -) OF PNRAT(PNRATM)
      AND THE DELAYED TIME OF THESE MAXIMA(TPRIM).
      * * * * *
      IF(PNRAT(I-1)-PNRAT(I))214,216,216C
214    IF(1SIGN)218C,215C,219C
215    IF(I-1)219C,215C,2155
      1SIGN = +1
      GO TO 219C
216    IF(1SIGN)219C,217C,218C
217    IF(I-1)219C,215C,2175
      1SIGN = -1
      GO TO 219C
218    MAXCT = MAXCT + 1
      PNRATM(MAXCT) = ABS(PNRAT(I-1))
      TPRIM(MAXCT) = TPRI(I-1)
      1SIGN = - 1SIGN
      CONTINUE
219    IF(I-9C)22,23,23
      I=I+1
      TPRI(I)=TPRI(I-1)+DELT
      NN=I-1
22    IF(TPRI(I)-TFMAX)3,3,23
      CALL NORM(PNRATM,MAXCT)
23    * * * * *
      THIS PORTION READS IN EXPERIMENTAL DATA
      * * * * *
      READ(5,62,1)N1,(ACXP(JJ),JJ=1,N1)
      FORMAT(I3,7X,7E10.0/(8E10.0))
620

```

[illegible]


```

1. RESULT=9.999999999E74
   RETURN
5  WRITE (6,107)
   STOP
6  IF(N0)5,7,7
7  J0=2*INT(X)
   MC=NC
   IF(M0-JC)11,12,12
11  M0=JC
12  M0=MC+11
   T(M0)=A.C
   LUB=M0-1
   T(LUB)=1.7F-74
   IF(KCODE)51,23,51
23  F=2.0*LUP
   M0=MC-3
   I2=M0
24  F=F-2.0
   T(I2+1)=F/X*T(I2+2)-T(I2+3)
   IF(I2)25,26,25
25  I2=I2-1
   GO TO 24
26  SUM=T(I1)
   DO 40 J=3,M0,2
40  SUM=SUM+2.*T(J)
   F=1./SUM
   DO 50 J=1,KC
50  T(J)=T(J)*F
   RETURN
51  F=2.*LUB-2.
   M0=MC-3
   I2=M0
511  T(I2+1)=F/X*T(I2+2)+T(I2+3)
   IF(I2)52,53,52
52  I2=I2-1
   F=F-2.
   GO TO 511
53  SUM=T(I1)
   DO 70 J=2,M0
70  SUM=SUM+2.*T(J)
   F=1./SUM*EXP(X)
   DO 80 J=1,KC
80  T(J)=T(J)*F
   RETURN
   END

```


XX

PROGRAM STEP INI

THIS PROGRAM GIVES GRAPHS OF THE ACOUSTIC PRESSURE(PNRAT) AT A POSITION (R-A) METERS FROM A CYLINDRICAL SOURCE OF RADIUS,A, METERS IN A PRESSURE RELEASE ISO-VELOCITY LAYER OF DEPTH,D, METERS AS A RESULT OF A STEP INPUT IN VELOCITY AT R-A=0 AT TIME,T,=0.

THE ACOUSTIC VARIABLES ARE OBTAINED BY EVALUATING TRIG APPROXIMATIONS TO THE ASYMPTOTIC APPROXIMATIONS OF THE BESSEL FUNCTIONS. PNPRAT CONSISTS OF A MAIN DUCT SOLUTION TERM, PNMAIN, AND A CORRECTION TERM, PNCOR. FOR THE LAYER, PNPRAT IS GRAPHED TO SHOW THE FULL SOLUTION FOR THE LAYER. AXIS CROSSINGS FOR PNPRAT AND PNMAIN ARE CALCULATED. THE MAXIMA (+) OF PNPRAT(PNPRATM) AND THE DELAYED TIME OF THESE MAXIMA (TPRIM OR -) OF PNPRAT(PNPRATM) ARE DETERMINED.

INPUT DATA

DATA FIELDS

ALL ELU.5

DATA DESCRIPTION (ALL MKS UNITS)

R=DISTANCE FROM RECEIVER TO CENTER OF TRANSMITTED
 A=RADIUS OF SOURCE
 DELT=INCREMENT OF TIME BY WHICH VALUES ARE
 GENERATED.
 TPTMAX=MAXIMUM DELAYED TIME FOR WHICH VALUES ARE
 GENERATED.
 C=SPEED OF SOUND IN LAYER.
 NFEN= NORMAL MODE NUMBER OF THE LAYER CONTRIBUTING
 TO VALUES.
 D=DEPTH OF WATER IN LAYER.
 0) FORMAT FOR EXPERIMENTAL DATA. I³ IS FORMAT
 FOR N1 AND N2 EXPLAINED BELOW. 7x SKIPS TO
 COLUMN 11 AND REMAINING FIELDS, ALL EIO.1,
 ON AS MANY CARDS AS ARE NEEDED FOR
 EXPERIMENTAL DATA.
 N1=NUMBER OF EXPERIMENTAL AXIS CROSSINGS IN
 PRESSURE.
 MACXP=EXPERIMENTALLY DETERMINED AXIS CROSSINGS
 IN PRESSURE.

```

CCCCCCCCCCCCCCCCCCCCCCCCCCCCCCCCCCCCCCCCCCCCCCCCCCCCCCCCCCCC
N2=NUMBER OF EXPERIMENTAL MAXIMA (+ OR -) IN
    PRESSURE.
AMPXP=EXPERIMENTALLY DETERMINED VALUES OF PEAK
    AMPLITUDES (+ OR -) IN PRESSURE.

OTHER VALUES

CPT= TIME OF FLIGHT OF SOUND FROM SOURCE TO RECEIVER AT POSITION R
WN=CUT-OFF FREQUENCY OF MODE NUMBER EN
TPRI=DELAYED TIME. THE TIME WHICH HAS ELAPSED AT A POSITION R SINCE
    THE TRANSIENT FIRST REACHED THAT POINT. TPRI WILL RUN FROM 0 TO
    TPMAX.
TVAL=SQRT((1-CPT)/(1+CPT))
ACOPM=COMPUTED AXIS CROSSING IN DUCT TERM,PNMAIN.
ACOPR=COMPUTED AXIS CROSSING IN PNRA.
ARG=WN*SQRT(1*2-CPT**2)
CYCLE=NUMBER OF CYCLES OF TRANSIENT GENERATED IN TIME TPRI.
CYCLEA=CYCLE NUMBER WHERE THEORY FAILS TO HOLD.
TPRIA=DELAYED TIME WHERE THEORY FAILS TO HOLD.
AMP=AMPLITUDE FACTOR DUE TO CORRECTION TO DUCT TERM(PNMAIN)
    BECAUSE OF LAYER EFFECT.
GAMMA=PHASE ANGLE IN AXIS CROSSINGS AS A RESULT OF CORRECTION
    TO DUCT TERM DUE TO LAYER EFFECT.
ARG1=ARGUMENT OF TRIG FUNCTION
PSI = PHASE ANGLE OF ACOPR
DELTA = ACOPM-ACOPR
DELTA1=MUM(ACXP-ACOPR)
A MAXIMUM OF 999 POINTS WILL BE CALCULATED AND PLOTTED.
* * * * *
DIMENSION ARG(999), TPRI(999), PNRA(999), CYCLE(999), RATIO(999),
1 AMP(999), ARG1(999), GAMMA(999), TVAL(999), AA(999), BR(999),
2 ACOPR(33), ACXP(33), PNRA(33), TPRI(33), AMPXP(33), TVAL1(33),
3 ARG2(33), EXN(33), RAT1(33), CC(33), DD(33), PSI(33), DELTA1(33),
4 PNMAIN(999), ARG3(999), ACOPM(33), DELTA(33)
REAL LABEL/4H
REAL*8 ITITLE(12)/,STEPIN1, A, B, J, ATFS, RO, X O, T,
1, PNRA, VS, TPRI, DELT=.4U, S, TPMAX=.36US R=,
2 JJ=0
KK=0
II=1
ISIGN = 1
MAXCT = 0
READ(5,2)R,A,DELT,TPMAX,C,EN,D

```

```

2  FORMAT(7E12.5)
3  IF(DEL T)200,200,201
4  STOP
5  CPT=(R-A)/C
6  ADOVERR=A/R
7  WN=(3.1415927*EN*C)/D
8  CAWN=C/(A*WN)
9  TSUBA = CPT*SQRT(1. + (1./CAWN)**2)
10 TPRIA=TSUBA-CPT
11 AC1=-(3./8. + 1./8.*ADOVERR)
12 BC1=33./128. + 6./128.*ADOVERR +9./128.*ADOVERR**2
13 FDGP=1.0
14 CYCLEA=(WN*CPT)/(6.2831854*CAWN)
15 I=1
16 TPRI(I)=0.0
17 TVAL(I)=SQRT(TPRI(I)/(TPRI(I) + 2.*CPT))
18 ARG(I) = 0.0
19 IF(TVAL(I) .NE. 0.0)ARG(I)=WN*TPRI(I)/TVAL(I)
20 CYCLE(I) = (ARG(I)/6.2831854)
21 RATIO(I)=CYCLE(I)/CYCLEA
22 AA(I)=-AC1*FATIO(I)
23 BB(I) = 1.-RC1*FDGP*RATIO(I)**2
24 AMPP(I)=SQRT(BB(I)**2 + AA(I)**2)
25 GAMMA(I) = ATAN2(AA(I),BB(I))
26 ARG1(I)=6.2831854*CYCLE(I)-(3.1415927/4.) + GAMMA(I)
27 ARG3(I)=6.2831854*CYCLE(I)-((3.*3.1415927)/4.)
28
29
30
31
32
33
34
35
36
37
38
39
40
41
42
43
44
45
46
47
48
49
50
51
52
53
54
55
56
57
58
59
60
61
62
63
64
65
66
67
68
69
70
71
72
73
74
75
76
77
78
79
80
81
82
83
84
85
86
87
88
89
90
91
92
93
94
95
96
97
98
99
100

```


[illegible]

PROGRAM STEP IN I

THESE ACOUSTIC VARIABLES ARE OBTAINED BY EVALUATING COMBINATIONS OF TRUNCATED INFINITE SUMS OF BESSEL FUNCTIONS. ZNRAT CONSISTS OF A MAIN DUCT SOLUTION TERM, ZNMAIN, AND A CORRECTION TERM, ZNCOR, FOR THE LAYER. ZNRAT IS GRAPHED TO SHOW THE FULL SOLUTION FOR THE LAYER. AXIS CROSSINGS FOR ZNRAT AND ZNMAIN ARE CALCULATED. THE MAXIMA (+ OR -) OF ZNRAT (ZNRATM) AND THE DELAYED TIME OF THESE MAXIMA (TPRIM) ARE DETERMINED.

INPUT DATA

DATA FIELDS

ALL E1v.5

DATA DESCRIPTION (ALL MKS UNITS)

```

ALL ELU.5
R=DISTANCE FROM RECEIVER TO CENTER OF TRANSMITTER
A=RADIUS OF SOURCE
DELT=INCREMENT OF TIME BY WHICH VALUES ARE
GENERATED.
TPMAX=MAXIMUM DELAYED TIME FOR WHICH VALUES ARE
GENERATED.
C=SPEED OF SOUND IN LAYER.
EN= NORMAL MODE NUMBER OF THE LAYER CONTRIBUTING
TO VALUES.
D=DEPTH OF WATER IN LAYER.
I3,7X,7F10.0 / (8E10.0) ) FORMAT FOR EXPERIMENTAL DATA. I3 IS FORMAT
FOR N3 AND N4 EXPLAINED BELOW. 7X SKIPS TO
COLUMN 11 AND REMAINING FIELDS. ALL E10.0,
ON AS MANY CARDS AS ARE NEEDED FOR
EXPERIMENTAL DATA.
N3= NUMBER OF EXPERIMENTAL AXIS CROSSINGS IN
PARTICLE DISPLACEMENT.
ACXZ=EXPERIMENTALLY DETERMINED AXIS CROSSINGS
IN PARTICLE DISPLACEMENT.

```

CC

N4= NUMRER OF EXPERIMENTAL MAXIMA (+ OR -) IN
PARTICLE DISPLACEMENT.
AMPXZ=EXPERIMENTALLY DETERMINED VALUES OF PEAK
AMPLITUDES (+ OR -) IN DISPLACEMENT.

OTHER VALUES

CPT= TIME OF FLIGHT OF SOUND FROM SOURCE TO PECEIVER AT POSITION R
WN=CUT-OFF FREQUENCY OF MODE NUMRER EN
TPRI=DELAYED TIME. THE TIME WHICH HAS ELAPSED AT A POSITION R SINCE
THE TPANSIENT FIRST REACHED THAT POINT. TPRI WILL RUN FROM 0 TO
TPMAX.
S= DUMMY QUANTITY FOR CALL RES SUBROUTINE.
TVAL =SQRT((T-CPT)/(T+CPT))
CRESUL=VALUE RES SUBROUTINE GIVES IN CALCULATING ZNMAIN.
DRESUL=VALUE RES SUBROUTINE GIVES IN CALCULATING ZNCOR.
ACQZM=COMPUTED AXIS CROSSINGS IN DUCT TERM,ZNMAIN.
ACQZR=COMPUTED AXIS CROSSINGS IN ZNRAT
AMPZM=AMPXZ/ZNPRAT
CYCLEA=CYCLE NUMBER WHERE THEORY FAILS TO HOLD.
TPRIA=DELAYED TIME WHERE THEORY FAILS TO HOLD.
A MAXIMUM OF 900 POINTS WILL BE CALCULATED AND PLOTTED.

DIMENSION S(500),ARG(900),TPRI(900),TVAL(900),ZNRAT(900),
1 ZNMAIN(900),ZNCOR(900),ZNCOR1(900),CRESUL(900),DRESUL(900),
2 ACQZM(50),ACQZR(50),ZNPATM(50),TPRIM(50),ACXZ(50),AMPZM(50),
3 AMPZM1(50),AMPXZ(50)
REAL LABEL/4H
REAL*8 TITLE(12)/,STEPIN1,.,.A,B,0.,,ATES,80.,,X0 B,.,
1 ZNRAT,.,,VS TPRI,.,,DELT=.4U,.,,S TPRAT=.0,.,,360US R=.,
2 ZNRAT,.,,VS TPRI,.,,DELT=.4U,.,,S TPRAT=.0,.,,360US R=.,

1 JJ=0
MAXCT=0
ISIGN=0

2 READ(5,2)R,A,DELT,TPMAX,C,EN,D
FORMAT(7E10.5)
IF(DELT)200,200,201
STOP
CPT=(R-A)/C
DCVERA=D/A
WN=(3.1415927*EN*C)/D

```

CAWN=C/(A*CWN)
TSUBA=CPRT*SQRT(1.+ (1./CAWN)**2)
TPRIA=TSUBA-CPT
CYCLEA=(WNCPT)/(6.2831854*CAWN)
AOVERR=A/R
A11=-3./8.+ 3./8.*AOVERR
B11=33./128.- 18./128.*AOVERR - 15./128.*AOVERR**2
CORR=2.*CAWN
FDGZ = 1.0)
I=1
TPRI(I)=C.0
TVAL(I)=SQRT(TPRI(I)/(TPRI(I)+2.*CPT))
ARG(I)=0.0
IF(TVAL(I).NE.0.C)ARG(I)=WNCPTPRI(I)/TVAL(I)

143 THIS PORTION EVALUATES ZNRAT,ZNMAIN,AND ZNCOR FROM THE FOLLOWING
EXPRESSION,
(ZNRAT*SQRT(R/A)*WN)/Z = 2*SUM(M=1 TO 10)(2M-1)*((T-CPT)/(T+CPT))**
((2M-1)/2)*JSUB(2M-1)(ARG) + CORR*A11*SUM(M=1 TO 10)2M*
((T-CPT)/(T+CPT))**M*JSUB(2M)(ARG) + 1/2*CRR**2*FDGZ*B11*
SUM(M=1 TO 10)(2M-1)*((T-CPT)/(T+CPT))**((2M-1)/2)*
JSUB(2M-1)(ARG) - SUM(M=1 TO 10)((-1)**(M-1))*((T-CPT)/(T+CPT))
**((2M-1)/2)*JSUB(2M-1)(ARG)
WHERE FDGZ = 1
A11 = -3/8 + 3/8*A/R
B11 = 33/128 - 18/128*A/R - 15/128*(A/R)**2

WHERE THE FIRST TERM IS ZNMAIN, REMAINDER
IS ZNCOR, AND ARG IS SAME AS BEFORE.

MO=20
TEMP=TVAL(I)
CALL RES(MC,ARG(I),O,CRESUL(I),S)
CSUM=TEMP*S(2)
SIGN=1.0
ESUM=CSUM
TFMP2=TEMP**2
DO 17 M=4,M0,2
TEMP=TFMP*TEMP2
SIGN=-SIGN
CSUM=CSUM+(M-1)*TEMP*S(M)
ESUM=ESUM+SIGN*TEMP*S(M)
17 CONTINUE

```



```

CALL DRAW (NN,TPRI,ZNRAT,G,G,LABEL,ITITLE,5.0E-05,5.0E-02,0,0,0,0,
1 C,9,15,0,L)
GO TO 1
END

```

```

SUBROUTINE RES(NG,X,KODE,RESULT,T)
FORMAT(55HNEGATIVE ORDER NOT ACCEPTED IN RESSEL FUNCTION ROUTINE)

```

107

```
KO=NO+1
```

```
IF(X)6,1,6
```

```
IF(NO)4,2,3
```

```
T(1)=1.0
```

```
RESULT=1.0
```

```
RETURN
```

```
IF(KC)5,10,2
```

```
RESULT=0.0
```

```
T(1)=0.0
```

```
RETURN
```

```
RESULT=9.99999999E74
```

```
RETURN
```

```
WRITE (6,107)
```

```
STOP
```

```
IF(NO)5,7,7
```

```
JO =2*INT(X)
```

```
MO=NC
```

```
IF(MO-JO)11,12,12
```

```
MO=JO
```

```
MO=MO+11
```

```
T(MO)=0.0
```

```
LUR=MO-1
```

```
Y(LUR)=1.0E-74
```

```
IF(KODE)51,23,51
```

```
F=2.0*LUR
```

```
MO=MO-3
```

```
I2=MO
```

```
F=F-2.0
```

```
T(I2+1)=F/X*T(I2+2)-T(I2+3)
```

```
IF(I2)25,26,25
```

```
I2=I2-1
```

```
GO TO 24
```

```
SUM=T(1)
```

```
DO 40 J=3,MO,2
```

```
SUM=SUM+2.0*T(J)
```

```
F=1.0/SUM
```

```
DO 50 J=1,KO
```

```
T(J)=T(J)*F
```

```
RESULT=T(KO)
```

```
RETURN
```

```

51 F=2.*LUR-2.
   MO=MC-3
   I2=MO
511 T(I2+1)=F/X*T(I2+2)+T(I2+3)
52 IF(I2)52,53,52
   I2=I2-1
   F=F-2.
   GO TO 511
53 SUM=T(1)
   DO 70 J=2,MC
70 SUM=SUM+2.*T(J)
   F=1./ (SUM*EXP(X))
   DO 80 J=1,KC
80 T(J)=T(J)*F
   RESULT=T(KC)
   RETURN
   END
SYNOPSIS NCR*(A,N)
J=1
DO 10 I=1,N
10 IF (ABS(A(J))-ABS(A(I)))5,10,10
   J=I
   CONTINUE
TEMP=A(J)
DO 20 I=1,N
20 A(I)= A(I)/TEMP
   RETURN
   END

```

```

* * * * * SAMPLE DATA CHECK FOR CNE RUN * * * * *
C C C C C
C 9.08E-01 6.00E-02 4.00E-07 3.60E-04 1.46972E03 1.00E-06 8.00E-02
C 13.00E-06 13.00E-06 25.73E-06 44.20E-06 64.14E-06 87.65E-06 115.76E-06
C 150.0E-06 185.38E-06 228.67E-06 269.23E-06 314.45E-06 354.12E-06
C 13 1.20E0 2.78E0 1.50E0 1.72E0 2.08E0 2.10E0 1.50E0
C 1.20E0 2.92E0 0.82E0 0.70E0 0.98E0 1.00E0
C 908M A=.0600M D=.0870M
C * * * * *

```

PROGRAM STEP IN I

THIS PROGRAM GIVES GRAPHS OF THE ACOUSTIC PARTICLE DISPLACEMENT, ZNRAT, AT A POSITION (R-A) METERS FROM A CYLINDRICAL SOURCE OF RADIUS, A, METERS IN A PRESSURE RELEASE ISO-VELOCITY LAYER OF DEPTH, D, METERS AS A RESULT OF A STEP INPUT IN VELOCITY AT R-A=C AT TIME, T, =.

THE ACOUSTIC VARIABLES ARE OBTAINED BY EVALUATING TRIG APPROXIMATIONS TO THE ASYMPTOTIC APPROXIMATIONS OF THE RESSEL FUNCTIONS. ZNRAT CONSISTS OF A MAIN DUCT SOLUTION TERM, ZNMAIN, AND A CORRECTION TERM, ZNCOR, FOR THE LAYER. ZNRAT IS GRAPHED TO SHOW THE FULL SOLUTION FOR THE LAYER. AXIS CROSSINGS FOR ZNRAT AND ZNMAIN ARE CALCULATED. THE MAXIMA (+) OR -) OF ZNRAT(ZNRATM) AND THE DELAYED TIME OF THESE MAXIMA (TPRM) ARE DETERMINED.

INPUT DATA

DATA FIELDS

ALL F10.5

DATA DESCRIPTION (ALL MKS UNITS)

```

ALL ELO.5
R=DISTANCE FROM RECEIVER TO CENTER OF TRANSMITTER
A=RADIUS OF SOURCE
DELT=INCREMENT OF TIME BY WHICH VALUES ARE
      GENERATED.
TPMAX=MAXIMUM DELAYED TIME FOR WHICH VALUES ARE
      GENERATED.
C=SPEED OF SOUND IN LAYER.
EN= NORMAL MODE NUMBER OF THE LAYER CONTRIBUTING
    TO VALUES.
D=DEPTH OF WATER IN LAYER.
      FORMAT FOR EXPERIMENTAL DATA. I3 IS FORMAT
      FOR N3 AND N4 EXPLAINED BELOW. 7X SKIPS TO
      COLUMN 11 AND REMAINING FIELDS, ALL ELO.0.
      ON AS MANY CARDS AS ARE NEEDED FOR
      EXPERIMENTAL DATA.
      N3= NUMBER OF EXPERIMENTAL AXIS CROSSINGS IN
            PARTICLE DISPLACEMENT.

```



```

MAXCT=0
ISIGN=0
READ(5,2)R,A,DELTA,TPMAX,C,EN,D
FORMAT(7E10.2)
IF(DELTA)200,200,201
STOP
CPT=(R-A)/C
ADOVER=A/R
WN=(3.1415927*EN*C)/D
CAWN=C/(A*WN)
TSUBA=CPT*SQRT(1.+(1./CAWN)**2)
TPRIA=TSUBA-CPT
CYCLEA=(WN*CPT)/(6.2831854*CAWN)
ALL=-3./8.+3./8.*ADOVER
R11=33./128.-18./128.*ADOVER-15./128.*ADOVER**2
FDGZ=1.
I=1
TPRI(I)=C.0
TVAL(I)=SQRT(TPRI(I)/(TPRI(I)+2.*CPT))
ARG(I)=C.0
IF(TVAL(I).NE.C.0)ARG(I)=WN*TPRI(I)/TVAL(I)
CYCLE(I)=(ARG(I)/6.2831854)
RATIO(I)=CYCLE(I)/CYCLEA
AA(I)=-ALL*RATIO(I)
BB(I)=1.-811*FDGZ*RATIO(I)**2
AMPZ(I)=SQRT(BB(I)**2+AA(I)**2)
GAMMA(I)=ATAN2(AA(I),BB(I))
ARG1(I)=6.2831854*CYCLE(I)-(3.1415927/4.)+GAMMA(I)
T(I)=TPRI(I)+CPT
ARG3(I)=6.2831854*CYCLE(I)-((3.*3.1415927)/4.)

THIS PORTION EVALUATES ZNRAT AND ZNMAIN FROM THE FOLLOWING
EXPRESSION:

ZNRAT*(SQRT(R/A)*WN)/Z=((1/3.1415927)*(1/SQRT(CYCLE(I)))*
AMPZ(I))*(CPT/(T(I)**2))*SQRT(ARG(I))*SIN(ARG1(I))

ZNMAIN IS CALCULATED BY SETTING AMPZ=1 AND LETTING PHASE
ANGLE IN ARG1=0.
IT ALSO DETERMINES IF AN AXIS CROSSING HAS OCCURRED IN ZNMAIN OR
ZNRAT TERM. IF SO, IT DETERMINES DELAY TIME(ACDZM OR ACDZR) AT
WHICH IT OCCURRED.

```



```

      GRAPH PLOTTING PORTION OF PROGRAM
      READ(5,37) ITITLE(10),ITITLE(11),ITITLE(12)
      FORMAT(3A8)
      CALL DRAW(NN,TPRI,ZNRAT,O,C,LABEL,ITITLE,5.0E-5,5.0E-12,0,0,0,
     1 C,9,15,0,L)
      GO TO 1
      END
      SUBROUTINE NCRM(A,N)
      J=1
      DO 10 I=1,N
      IF (ABS(A(J))-ABS(A(I))) 5,10,10
      J=I
      CONTINUE
      TEMP=A(J)
      DO 20 I=1,N
      A(I)=A(I)/TEMP
      RETURN
      END

```

[illegible]

INITIAL DISTRIBUTION LIST

	No. Copies
1. Defense Documentation Center Cameron Station Alexandria, Virginia 22314	20
2. Library Naval Postgraduate School Monterey, California 93940	2
3. Chief of Naval Research Office of Naval Research Washington, D. C. 20360	1
4. Professor Alan B. Coppens Department of Physics Naval Postgraduate School Monterey, California 93940	7
5. Professor Raymond L. Kelly Department of Physics Naval Postgraduate School Monterey, California 93940	1
6. Professor W. P. Cunningham Department of Physics Naval Postgraduate School Monterey, California 93940	2
7. LT Anthony B. Oates Class 25 Naval Destroyer School Newport, Rhode Island 02840	2
8. Mr. William E. Smith Department of Physics Naval Postgraduate School Monterey, California 93940	1

UNCLASSIFIED

Security Classification

DOCUMENT CONTROL DATA - R & D

Security classification of title, body of abstract and indexing annotation must be entered when the overall report is classified)

1 ORIGINATING ACTIVITY (Corporate author) Naval Postgraduate School Monterey, California 93940		2a. REPORT SECURITY CLASSIFICATION <u>Unclassified</u>	
		2b. GROUP	
3 REPORT TITLE Propagation of a Simple Transient in an Isovelocity Layer with Pressure-Release Boundaries			
4 DESCRIPTIVE NOTES (Type of report and, inclusive dates) Master of Science thesis, June 1968			
5 AUTHOR(S) (First name, middle initial, last name) Anthony Brent Oates			
6 REPORT DATE June 1968		7a. TOTAL NO. OF PAGES 94	7b. NO. OF REFS 17
8a. CONTRACT OR GRANT NO.		9a. ORIGINATOR'S REPORT NUMBER(S)	
b. PROJECT NO.			
c.		9b. OTHER REPORT NO(S) (Any other numbers that may be assigned this report)	
d.			
10. DISTRIBUTION STATEMENT This document is subject to special export controls and each transmittal to foreign government or foreign nationals may be made only with prior approval of the Naval Postgraduate School.			
11. SUPPLEMENTARY NOTES		12. SPONSORING MILITARY ACTIVITY	

13 ABSTRACT The propagation of a simple acoustic transient in an isovelocity water layer was investigated for the purpose of studying the region of validity of a suggested correlation between exact solutions in ducts and solutions for propagation in a layer. The Laplace transform method was used to obtain approximate solutions for the acoustic pressure, particle velocity, and particle displacement resulting from a step-function input in velocity. The radiation impedance characteristics of a Mylar transducer were investigated to study their effect on the received waveforms. Computer programs were written to evaluate and graph the resulting waveforms. The waveforms resulting from a step-function input in velocity were observed and compared with the predicted waveforms. With the use of a family of Mylar transducers, a somewhat doubtful correlation was obtained in the region of validity of the theoretical solutions. Possible causes of the disagreement between the theory and the experiment were investigated. It was found that the theory is believed to be correct, that the experiment was not accurate enough, and that further investigations should be conducted to study the assumed pressure-release characteristics of 1/4 inch polyethylene.
--

UNCLASSIFIED

Security Classification

14

KEY WORDS

LINK A

LINK B

LINK C

ROLE

WT

ROLE

WT

ROLE

WT

Acoustic Transients
Isovelocity Layer
Mylar Transducers
Barium Titanate Transducers
Laplace Transform
Pressure-Release Boundaries
Radially-Symmetric Propagation



thes0164

Preparation of a simple transcript

DUDLEY KNOX LIBRARY



3 2768 00421943 6

DUDLEY KNOX LIBRARY